AN EXPERIMENTAL INVESTIGATION OF THE EFFECTS OF SWIRLING AND PULSING THE FLOW THROUGH AN AXISYMETRIC DUCT

David Cornell Leestma

Naval Postgraduate School
Monterey, California

December 1972

NAVAL POSTGRADUATE SCHOOL
Monterey, California

THESIS

AN EXPERIMENTAL INVESTIGATION OF THE EFFECTS OF SWIRLING AND PULSING THE FLOW THROUGH AN AXISYMMETRIC DUCT

by

David Cornell Leestma

Thesis Advisor: G. J. Hokenson

December 1972

Approved for public release; distribution unlimited.

Security Classification

DOCUMENT CONTROL DATA - R & D

(Security classification of title, body of abstract and indexing annotation must be entered when the overall report is classified)

1. ORIGINATING ACTIVITY (Corporate author) Naval Postgraduate School Monterey, California 93940	2a. REPORT SECURITY CLASSIFICATION Unclassified 2b. GROUP

3. REPORT TITLE

AN EXPERIMENTAL INVESTIGATION OF THE EFFECTS OF SWIRLING AND PULSING THE FLOW THROUGH AN AXISYMMETRIC DUCT

4. DESCRIPTIVE NOTES (Type of report and, inclusive dates)

Master's Thesis; December 1972

5. AUTHOR(S) (First name, middle initial, last name)

David Cornell Leestma

6. REPORT DATE December 1972	7a. TOTAL NO. OF PAGES 108	7b. NO. OF REFS 14
8a. CONTRACT OR GRANT NO. b. PROJECT NO. c. d.	9a. ORIGINATOR'S REPORT NUMBER(S) 9b. OTHER REPORT NO(S) (Any other numbers that may be assigned this report)	

10. DISTRIBUTION STATEMENT

Approved for public release; distribution unlimited.

11. SUPPLEMENTARY NOTES	12. SPONSORING MILITARY ACTIVITY Naval Postgraduate School Monterey, California 93940

13. ABSTRACT

It is known that the presence of swirl in a flow stream can affect heat and mass transfer rates, and pulsatile flow has important aspects in physiological studies and in non-steady turbulent flows. ~~This~~ investigation consisted of an experimental study of the generation and decay of swirling flow in a duct utilizing a new method of swirl generation, and the measurement of the fluctuations imposed on the steady turbulent flow profile by pulsing the flow in a duct. New results were obtained that gave insight into the effects of swirling and pulsing the flow through an axisymmetric duct.

DD FORM 1 NOV 68 1473 (PAGE 1)

S/N 0101-807-6811

I

UNCLASSIFIED

Security Classification

A-31408

14. KEY WORDS	LINK A		LINK B		LINK C	
	ROLE	WT	ROLE	WT	ROLE	WT
Axisymmetric Duct						
Pulsing Flow						
Swirling Flow						

An Experimental Investigation of the Effects of Swirling and Pulsing the Flow Through an Axisymmetric Duct

by

David Cornell Leestma
Ensign, United States Navy
B.S.Ae.E., United States Naval Academy, 1971

Submitted in partial fulfillment of the

requirements for the degree of

MASTER OF SCIENCE IN AERONAUTICAL ENGINEERING

from the

NAVAL POSTGRADUATE SCHOOL
December 1972

Author David Cornell Leestma

Approved by: Gustave Hakeman
Thesis Advisor

R. W. Bellaye
Chairman, Department of Aeronautical Engineering

Milton U. Clauser
Academic Dean

ABSTRACT

It is known that the presence of swirl in a flow stream can affect heat and mass transfer rates, and pulsatile flow has important aspects in physiological studies and in non-steady turbulent flows. This investigation consisted of an experimental study of the generation and decay of swirling flow in a duct utilizing a new method of swirl generation, and the measurement of the fluctuations imposed on the steady turbulent flow profile by pulsing the flow in a duct. New results were obtained that gave insight into the effects of swirling and pulsing the flow through an axisymmetric duct.

TABLE OF CONTENTS

LIST OF TABLES

LIST OF FIGURES

List of Figures (Cont.)

I. INTRODUCTION

Turbulent flows are encountered in almost every application where fluid motion is involved. The case of turbulent flow through pipes has been investigated very thoroughly in the past due to its great practical importance. Moreover, the results obtained are not only important to pipe flow, but also greatly contribute to the fundamental knowledge of turbulent flows in general.

Classical laminar pipe flow theory was first developed by Hagen [1] and Poiseuille [2]. A fluid is accelerated through a pipe under the influence of a pressure gradient which acts in the direction of the axis and is retarded by the frictional shearing stress. At a sufficiently large distance from the entrance section the velocity distribution across the section becomes independent of the coordinate along the direction of flow and is given by

$$u(y) = \frac{P_1 - P_2}{4\mu l}(R^2 - y^2) \qquad (1)$$

The velocity is distributed parabolically over the radius and the maximum velocity occurs where $y = 0$. The volume flow rate is found to be

$$Q = \frac{R^4\pi}{8\mu l}(p_1 - p_2) \qquad (2)$$

Equation (2) is known as the Hagen-Poiseuille equation of laminar flow through a pipe.

The relationship between the pressure gradient and the rate of flow (eqn. (2)) could be determined theoretically for the case of laminar flow and the results agree well with experiment. However, in the case of turbulent flow such a relationship can only be obtained empirically. Reynolds [3], Blasius [4] and Prandtl [5] have all developed semi-empirical hypotheses for the case of fully developed turbulent flow. Blasius established the following empirical equation for the frictional resistance (λ) of smooth pipes of circular cross-section:

$$\lambda = 0.3164 \left(\frac{\bar{u}d}{\nu}\right)^{-1/4} \qquad (3)$$

Prandtl's universal law of friction for smooth pipes is

$$1/\sqrt{\lambda} = 2.0 \log \left(\frac{\bar{u}d\sqrt{\lambda}}{\nu}\right) - 0.8 \qquad (4)$$

Equations (3) and (4) were verified up to a Reynolds number of 3.4×10^6 by Nikuradse [6].

When a fluid enters a circular pipe the velocity distribution in cross-sections of the inlet length varies with the distance from the initial cross-section. In sections close to the inlet the velocity distribution is nearly uniform. Further downstream the velocity distribution changes due to the influence of friction until a fully developed velocity profile is attained at a given cross-section and remains constant downstream of it. The development length in turbulent flow is considerably shorter than in laminar flow. Nikuradse determined that the fully developed velocity profile exists

after an inlet length of 25 to 40 diameters, whereas for laminar flow the inlet length ranges from 150 to 300 pipe diameters.

The introduction of swirl into the flow through a pipe alters the characteristics of the flow. It is known that swirling flow increases heat and wall mass transfer rates as well as decreasing the mass flux through the system. Several investigators have attempted to formulate the problem of swirling flow by solving the complete Navier-Stokes equations. Many of these studies are discussed in the works of Murthy [7], Lavan and Fejer [8], Rochino and Lavan [9], and Farquhar, Norton and Hoffman [10, 11].

The study of swirling flows is of significant importance not only because it is a fundamental fluid flow phenomenon (vertex phenomena are found in nature in all scales, from the eddys that form the basis for turbulence to hurricanes and cyclones), but also because of its far-reaching applications. In gaseous nuclear reactor rocket motors, swirling motion may be utilized to achieve prolonged hold-up time of the fissionable gas. In plasma generators the swirling flow stabilizes the arc distance and offers thermal protection to the chamber walls due to the increase in the heat transfer rate. In certain combustion devices the swirling motion of the gases improves stability and combustion efficiency while reducing the heat loss through the walls. Swirling flows are also used for the separation of particles, as cooling devices

(i.e., Ranque-Hilsch tube), for regulating rocket thrust and other applications.

In many practical situations flow in ducts will have pressure gradient fluctuations. The theory for flow through a pipe under the influence of a periodic pressure gradient was first given by Sexl [12] and Uchida [13]. A recent study of randomly fluctuating pressure gradients was conducted by Perlmutter [14]. Pulsing flows through pipes have long been of interest in regards to the circulation system of the blood, and recently theories of pulsating flow are being applied to the super-charging system of reciprocating engines and the surging phenomena in power plants.

This investigation has been conducted to determine the effects of a new method of swirl generation on the turbulent flow profiles in a duct at several locations downstream from the swirl generator, and to measure the decay of the swirl and the distortion of the mean flow by the use of X-array hot-wire anemometry. Velocity profiles at several axial stations were obtained for periodically pulsating flow and compared with the theoretical results of Uchida.

II. EXPERIMENTAL APPARATUS

The experimental apparatus used in this investigation was designed and constructed to permit the study of swirling and pulsing turbulent flow through an axisymmetric duct. Briefly, the equipment generates swirling or pulsing flow in a pipe and provides for continuously variable swirl velocities or pulse amplitudes. Figure 1 is a picture of the experimental setup. The details of the equipment are discussed below.

A nozzle with quarter-elliptical wall contour was fabricated from 65% powdered aluminum-fill epoxy resin. It converged from an outside diameter of 32" to the eight-inch diameter of the duct in a length of 22 inches. Six static pressure taps were located on the nozzle wall. The entrance to the nozzle was fitted with a 32-inch diameter, four inch thick, one-quarter inch honeycomb mest mounted on three rollers. The honeycomb was inserted to reduce vortex motion and to establish parallel flow. A driving roller was pully-driven by a Vickers hydraulic transmission coupled to a Craftsman 1/2-HP motor to make the honeycomb structure rotate at variable angular velocities. The rotation of the honeycomb structure imparts a tangential velocity component into the flow and thus acts as a swirl generator (Fig. 2a). The outside edge of the structure was sealed by a felt lining to prevent air leaks into the nozzle behind the swirl generator (Fig. 2).

The duct was constructed of ten sections of eight inch diameter (7-7/8" inside diameter) extruded and reamed aluminum pipe, each section being four feet long. They were coupled by cork collars and clamped together. A final plastic section of the same dimensions connected the duct to the blower which allowed for observation of the damper motion. Forty static pressure taps were drilled into the duct and spaced one foot apart starting six inches from the exit of the nozzle. The duct was supported by ten cradling pods, each adjustable in height, so that the entire duct could be aligned and leveled (Fig. 3). An inclined water manometer was connected to the wall static pressure taps and set at an angle of 30° to provide a sensitivity increase of a factor of two (Fig. 4).

Air was drawn through the system by a Navy Standard centrifugal fan driven by a 3-HP, 3-phase continuous speed Baldour electric motor (Fig. 5). The flow rate was controlled by a damper in the duct located at the blower entrance. The damper could be positioned and set at any angle from fully open to full closed. It was connected by a rod to a flywheel turned by a Vickers hydraulic transmission driven by a Craftsman 1/2-HP capacitor motor to allow for a fluctuating mass flow through the system. The rod could be positioned at various radii from the center of the flywheel to give varying amplitudes to the damper. Varying the speed

of the hydraulic drive varies the frequency of oscillation of the mean flow through the duct. A gear-driven pot was attached to the damper arm to provide a reference wave form on the oscilloscope for the pulsating flow velocity profiles (Fig. 6).

Once the system was constructed, data was taken with a Thermo-Systems model 1050 constant temperature linearized anemometer in conjunction with a model 1015C correlator. They were used with two X-array hot-wire probes to measure U, V and V_θ velocities. The two probes were identical except the plane of the two wires on one was rotated 90° from the other so that all three velocity components could be measured by means of the two probes (Fig. 7). A one psi Stratham static pressure transducer was used to measure the wall static pressure fluctuations caused by the pulsing flow. The readings were recorded on Polaroid film by photographing the signal on an oscilloscope.

III. EXPERIMENTAL PROCEDURE

The basic experimental procedure used during this investigation began with dynamic pressure readings at one-half inch intervals radially from the wall of the duct to the centerline using a Prandtl-type calibrated pitot-static probe. These readings were taken at each of the three experimental stations (see below) for flow without swirl or pulsation to provide a reference for the calibration of the X-array hot-wire probes (see Appendix A). The X-array hot-wire probe was then inserted in the duct and the anemometer properly zeroed. Then, with the probe located at the center-line of the duct, the linear span on the anemometer was adjusted to give the desired voltage range. This was done with steady flow through the duct with no swirl or pulsation to provide the velocity voltage reference at each station.

The swirl generator and damper were then adjusted to give the desired flow conditions in the duct. Experimental measurements were made at three stations along the duct: Station #1 was located three pipe diameters from the exit of the nozzle; Station #2 was 21 pipe diameters from the nozzle exit; and Station #3 was 39 pipe diameters from the nozzle exit. At each station measurements were taken at one-half inch radial intervals from the wall to the center-line of the duct. Swirl measurements were obtained from the correlator on a digital read-out voltmeter. Voltage

readings were recorded for E_a+E_b and E_a-E_b for the hot-wire probes. These voltages were reduced to velocities by use of the calibration equations obtained for the probes (see Appendix A). For pulsing flow measurements, the output from the pot on the damper arm was displayed on the lower beam of a dual-beam oscilloscope and the hot-wire anemometer output to the upper beam. The outputs were then recorded on Polaroid film by photographing the signals on the oscilloscope. The same technique was used to record the wall static pressure data with the output of the static pressure transducer displayed on the upper beam of the oscilloscope.

IV. RESULTS AND DISCUSSION

This experimental study of swirling and pulsing flow in a duct produced a number of new and interesting results. The data from the experiment are tabulated in Appendices B, C, D, E and F. and are presented in graphical form on Figures 10 through 29. Results were obtained for two rates of swirl generation (corresponding to swirl generator velocities of 60 and 100 RPM) and for two different amplitudes of pulsation. The radial distribution of both the axial and tangential velocities was measured at three stations downstream located at three, 21 and 39 pipe diameters from the nozzle exit corresponding to entrance, developing, and nearly fully developed flow. At each station measurements were taken at one-half inch radial intervals from the wall to the centerline of the duct.

Figures 10, 11 and 12 show a comparison of the axial velocity profiles for the two rates of swirl with the steady flow profile. It can be seen that the swirl distorts the axial velocity profile from the steady flow case, filling the profile out near the wall of the duct. The swirling component of the velocity tends to keep the same shape as it moves downstream. The greater the swirl, the longer the flow retains its initial shape. It can also be seen that there is some distortion of the steady axial flow as it exits the nozzle (Station #1). The axial velocity profile has a bulge near

the wall of the duct which indicates that the nozzle is not uniformly accelerating the flow on each streamline as it passes through the nozzle.

Figures 13, 14 and 15 show a comparison of the average axial velocity profiles for two amplitudes of pulsating flow with the steady flow profile. The larger amplitude pulsation distorts the flow shape more than the small amplitude pulse. Again, the average pulsing flow does not proceed toward a fully developed flow profile as quickly as the steady flow. Note also the bulge effect near the wall at Station #1 that was also observed with the swirling flow.

Figures 16, 17 and 18 depict the axial velocity for the two rates of swirl and the steady flow as a function of radial distance into the duct. As the flow exits the nozzle the presence of swirl gives a larger axial velocity than the steady flow. The higher the rate of swirl, the greater the increase in the axial velocity. However, as the flow moves downstream, the axial velocity for the swirling flow does not increase as rapidly as for the steady flow, and soon is at a lower value than in the steady case. Near the wall the swirling flow has a greater axial velocity than the steady flow as the flow moves downstream.

The axial velocity data were replotted on Figures 19, 20 and 21 (which present the respective steady flow and two rates of swirl for all three stations) to facilitate a graphical integration to determine the volume flow rates (V).

By use of the equation

$$V = 2 \int_0^{r_o^2} (r/r_o) u d(r/r_o) \qquad (1)$$

the volume flow rates tabulated in Table I were obtained. It was found that an increase in the swirl velocity decreased the volume flow rate slightly.

The pulsing flow fluctuations were obtained by cycling the damper at a rate of one cycle every two seconds, or about 60 pulses per minute. From the Polaroid photographs of the pulsing flow (see Appendix D) the mean flow velocities for both amplitudes of pulsation were obtained at the measured radial positions in the duct and tabulated in Tables II, III and IV. For the small amplitude pulsation the axial flow velocities fluctuated approximately 14-18 ft/sec above and below the mean flow velocity, with the larger fluctuations occurring at Station #3. For the larger amplitude pulsation the axial flow velocities fluctuated approximately 23-25 ft/sec about the mean velocity, and this remained essentially the same for all three stations in the duct. The deviations from the mean velocity remained about the same magnitude at all the radial positions in the duct at each station for both large and small pulsation amplitudes. It was noted that the damper did not oscillate quite symmetrically for the large amplitude pulsation with the consequent slight differences between the minimum flow velocities for two consecutive pulses.

The average axial velocities for the pulsing flow were obtained by taking the average value from the oscilloscope. Figures 22 and 23 show that the centerline flow velocities increase while the flow velocities near the wall decrease as the flow moves downstream. The velocities for the small amplitude pulse are significantly greater than for the larger amplitude pulse, but both are less than for the steady flow. A graphical integration of the curves shows that the volume flow rates for the pulsing flow are greatly reduced from the steady flow case (see Table I). The data for Station #3 indicated that the flow velocity decays at about the same rate for both large and small amplitude pulsation.

A measure of the accuracy of the experimental measurements was also obtained from Table I. The volume flow rates were obtained at each downstream station for each of the flow conditions. Since the mass flow through the duct must be conserved, a comparison of these flow rates between stations for each type of flow gives a good indication of the accuracy of the data. The volume flow rates at each station were found to be within 1% of the mean flow rate for all types of flow.

Figures 24 and 25 show the tangential velocities as a function of radial distance. The curves are essentially straight lines and indicate that the solid body rotation initiated by the honeycomb has persisted. The tangential velocities show a tendency to decay faster near the centerline of the duct than near the wall. Also, the smaller rate

of swirl decays at a faster rate than the larger swirl. Figures 26 and 27 show the angular velocities as a function of the radial distance into the duct. The curves show a definite hump near the centerline which decays as the flow moves downstream. The bulge is more pronounced with the higher velocity swirl.

The average wall static pressure data obtained on the manometer are plotted on Figure 28 and show that the static pressure change for the larger swirl has a greater slope as the flow moves downstream. It starts as a smaller pressure drop than the steady flow and becomes a larger pressure drop as the flow moves downstream. The curves all indicate that the pressure drop is essentially a linear function of distance downstream. Figure 29 shows that the average wall static pressure drop is significantly reduced when the flow is pulsed, but still remains nearly linear with downstream distance.

The wall static pressure fluctuations for pulsing flow are shown in Appendix F. From the photographs it can again be seen that the damper was not oscillating quite symmetrically for the large amplitude pulsations. The wall static pressure fluctuations are observed to not give a regular periodic shape under the influence of the regular flow pulsations. These pressure profiles indicate the presence of some non-linearities imposed on the flow by the pulsation.

Velocity measurements were also obtained for the radial velocity component of the flow with pulsation (see Appendix D). It was found that there was a periodic oscillation in the radial velocity that increased in magnitude with axial distance downstream in the duct. The mean radial velocity was very small and averaged only 1-3% of the mean axial velocity.

V. CONCLUSIONS

The results of this experimental investigation of swirling and pulsing flow in an axisymmetric duct justify the following conclusions:

1. The new method of generating swirl used in this experiment effectively introduced a tangential component of velocity into the flow through the duct. The capability of adjusting the rotation rate of the swirl generator can be of great value when studying the effects on the flow of varying swirl velocities. The swirl generator can be used at speeds up to 120 RPM and provides a unique method of swirl generation at those rotation rates.

2. The presence of a swirl component in the flow through a pipe will produce a reduction in the mass flow rate through the duct. The presence of a periodic pulsating flow will significantly reduce the mass flow rate.

3. The swirl velocity decays at a faster rate near the centerline of the duct than near the wall. The smaller the swirl component of velocity, the faster the rate of decay of the swirl.

4. Both swirling and pulsing flows do not proceed toward a fully developed flow profile as rapidly as steady flow.

5. The analytic study by Uchida shows that a maximum of velocity distribution exists near the wall for laminar flow with high frequency periodic fluctuations. This velocity

bulge was not observed in this experiment due to the relative slow pulsation rate used and the fact that the flow was turbulent.

6. The presence of pulsation in the flow through a pipe distorts the wall static pressure profile by imposing non-linearities on the flow.

7. The presence of a periodically pulsating flow induces a small periodic radial velocity component into the flow.

TABLE I

VOLUME FLOW RATES

Flow Type	Station #1 ^3V (ft^3/sec)	Station #2 ^3V (ft^3/sec)	Station #3 ^3V (ft^3/sec)	Vave. (ft^3/sec)
Steady Flow	29.57	29.81	29.83	29.74
Large Swirl	29.34	29.22	29.29	29.28
Small Swirl	29.45	29.52	29.43	29.47
Large Pulse	17.72	17.68	17.50	17.63
Small Pulse	22.68	23.25	22.85	22.93

TABLE II

MEAN AXIAL FLOW VELOCITIES FOR PULSING FLOW - STATION #1

r/r_o	Small Amplitude $\bar{U}$ (ft/sec)	Small Amplitude $\bar{U}/\bar{U}_{\ell}$	Large Amplitude $\bar{U}$ (ft/sec)	Large Amplitude $\bar{U}/\bar{U}_{\ell}$
0.937	65.47	0.971	52.37	0.958
0.873	67.74	1.00	52.37	0.958
0.746	67.74	1.00	52.37	0.958
0.492	67.74	1.00	54.64	1.00
0.238	67.74	1.00	54.64	1.00
0.00	67.74	1.00	54.64	1.00

TABLE III

MEAN AXIAL FLOW VELOCITIES FOR PULSING FLOW - STATION #2

r/r_o	Small Amplitude $\overline{U}$ (ft/sec)	Small Amplitude $\overline{U}/\overline{U}_{\ell}$	Large Amplitude $\overline{U}$ (ft/sec)	Large Amplitude $\overline{U}/\overline{U}_{\ell}$
0.937	59.39	0.760	50.01	0.864
0.873	64.14	0.821	51.64	0.892
0.746	68.76	0.880	51.64	0.892
0.619	73.51	0.941	53.14	0.918
0.492	73.51	0.941	53.14	0.918
0.365	75.02	0.960	54.76	0.946
0.238	76.64	0.981	56.26	0.972
0.111	78.14	1.00	56.26	0.972
0.00	78.14	1.00	57.89	1.00

TABLE IV

MEAN AXIAL FLOW VELOCITIES FOR PULSING FLOW - STATION #3

r/r_o	Small Amplitude $\bar{U}$ (ft/sec)	Small Amplitude $\bar{U}/\bar{U}_{\ell}$	Large Amplitude $\bar{U}$ (ft/sec)	Large Amplitude $\bar{U}/\bar{U}_{\ell}$
0.937	58.95	0.795	45.55	0.773
0.873	63.02	0.797	48.23	0.818
0.746	66.99	0.847	50.91	0.864
0.619	71.06	0.898	53.59	0.909
0.492	75.03	0.949	56.27	0.955
0.365	76.42	0.966	56.27	0.955
0.238	77.71	0.982	57.56	0.976
0.111	79.10	1.00	57.56	0.976
0.00	79.10	1.00	58.95	1.00

FIGURE 1. EXPERIMENTAL SETUP

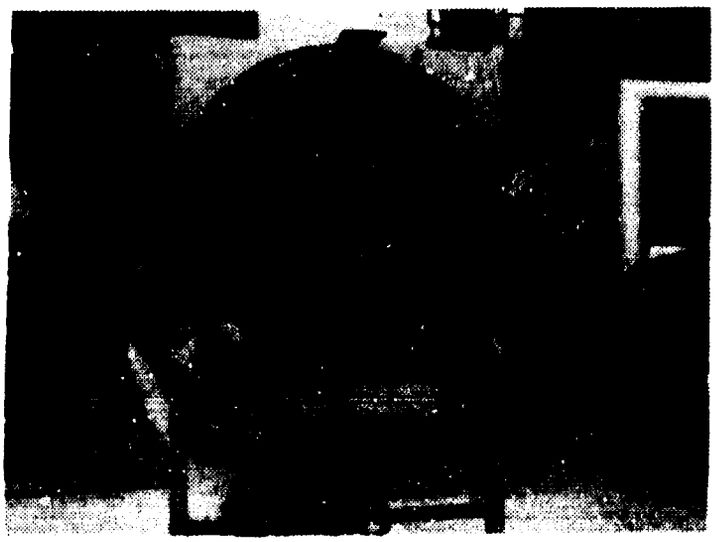

FIGURE 2. SWTRI GENERATOR

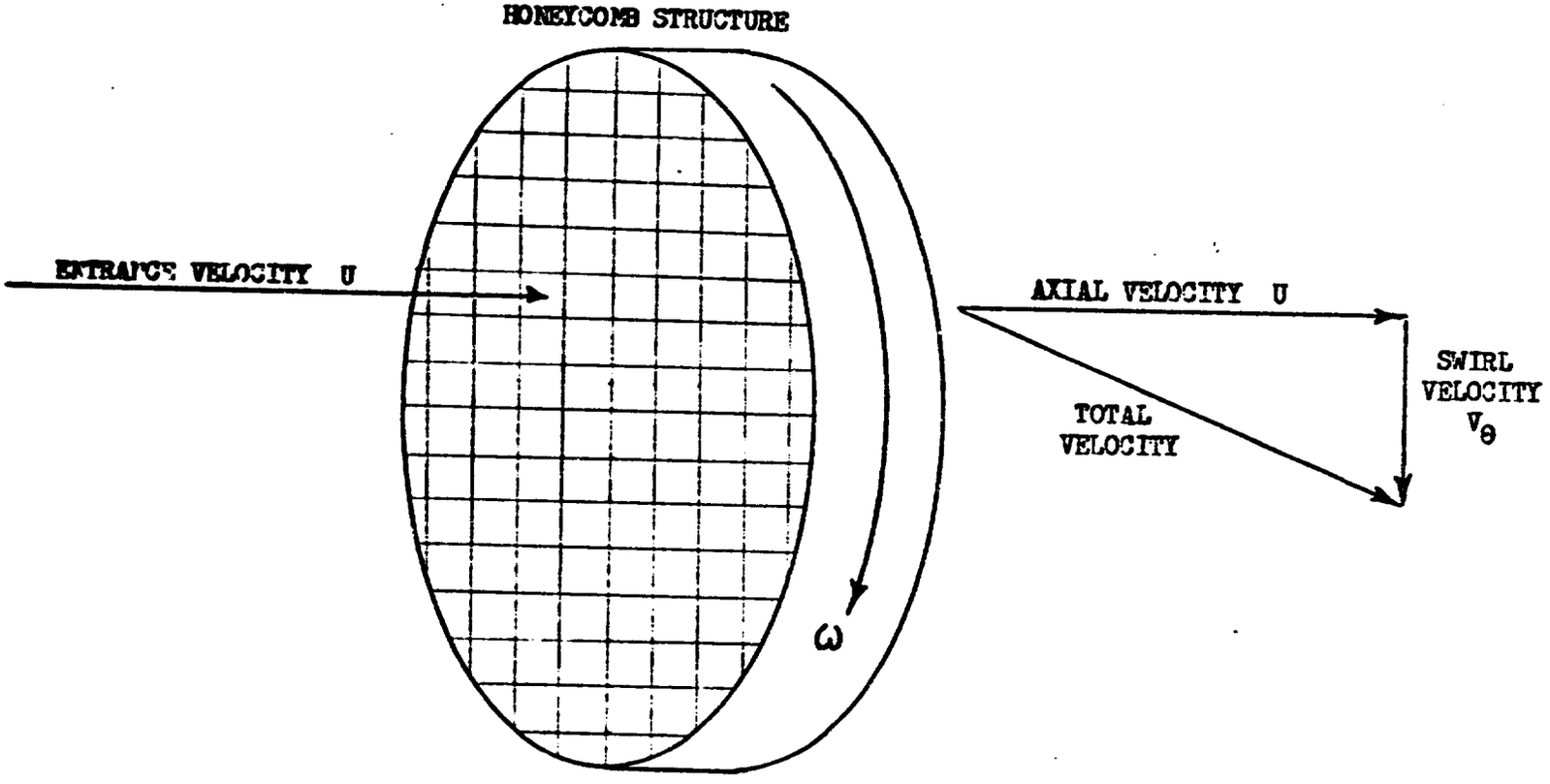

FIGURE 2a. SWIRL GENERATION DIAGRAM

FIGURE 3. EXPERIMENTAL DUCT

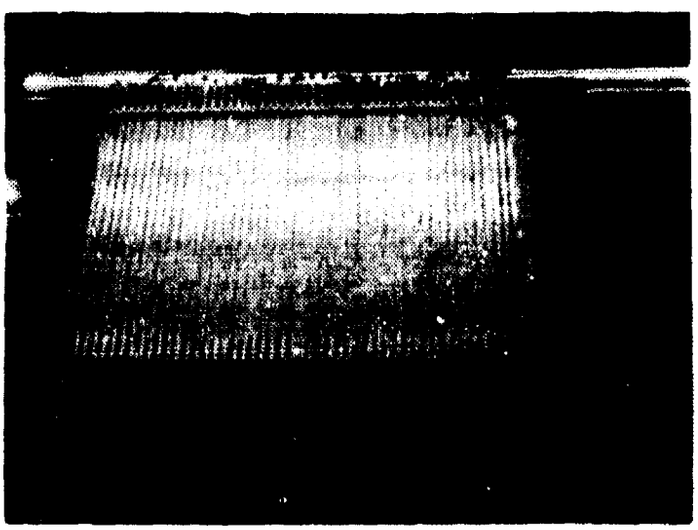

FIGURE 4. MANOMETER

FIGURE 5. CENTRIFUGAL FAN

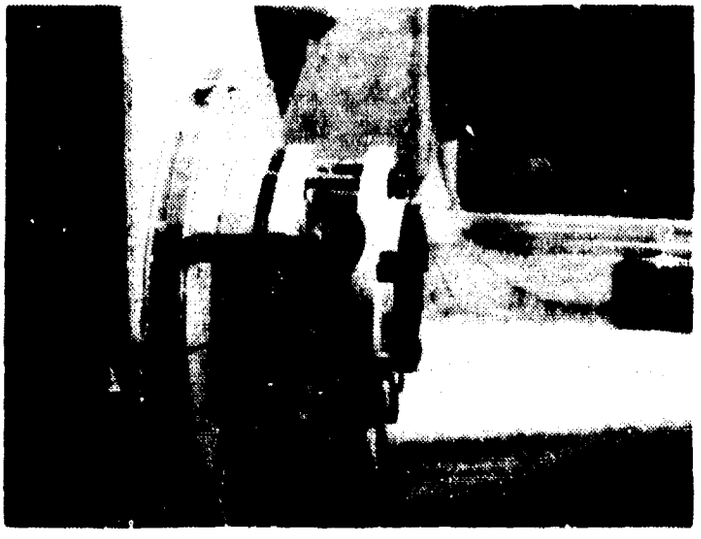

FIGURE 6. GEAR-DRIVEN DAMPER POT

FIGURE 7. HOT WIRE PROBE INSERTED INTO DUCT

FIGURE 8. X-ARRAY HOT WIRE PROBES

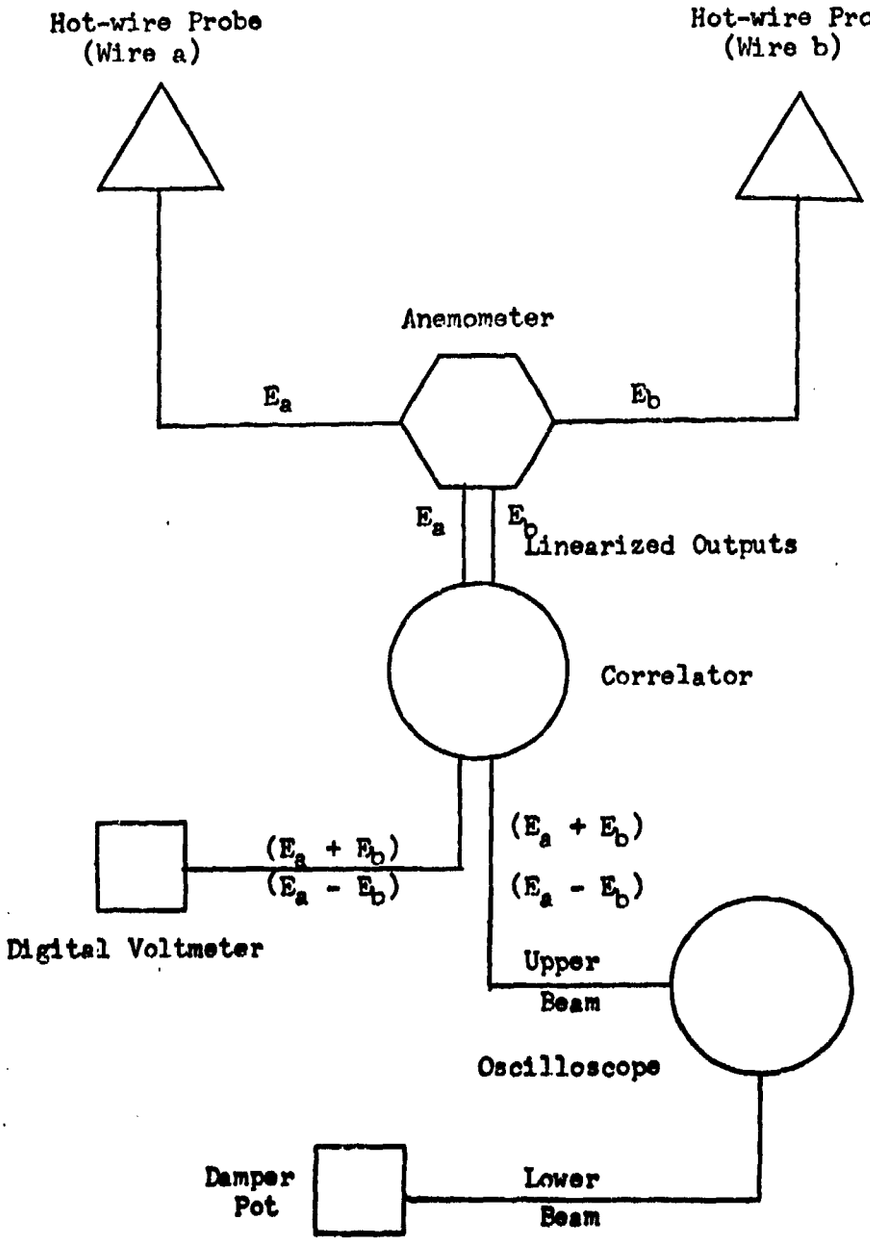

FIGURE 9. EXPERIMENTAL INSTRUMENTATION

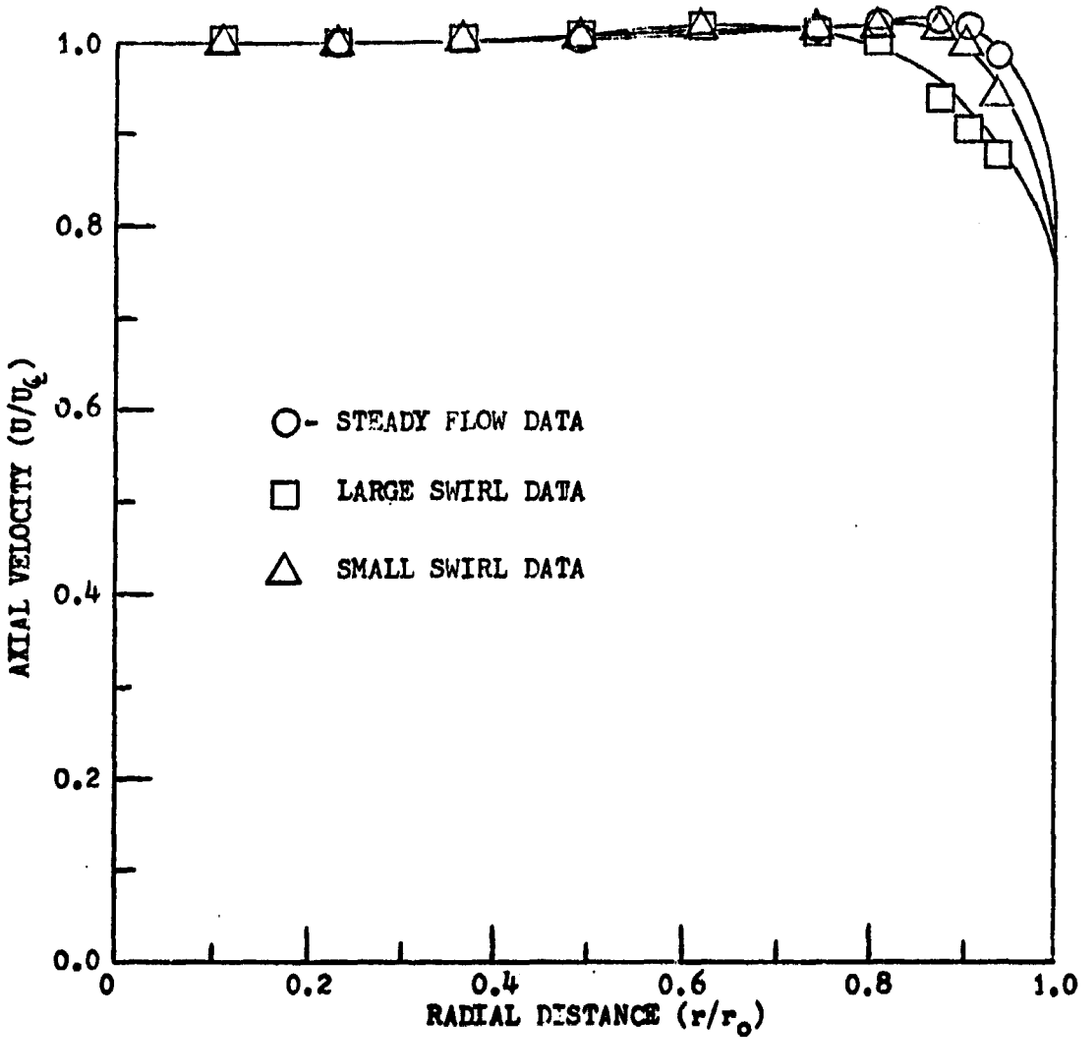

FIGURE 10. RADIAL DISTRIBUTION OF AXIAL VELOCITY AT STATION #1 FOR STEADY AND SWIRLING FLOW

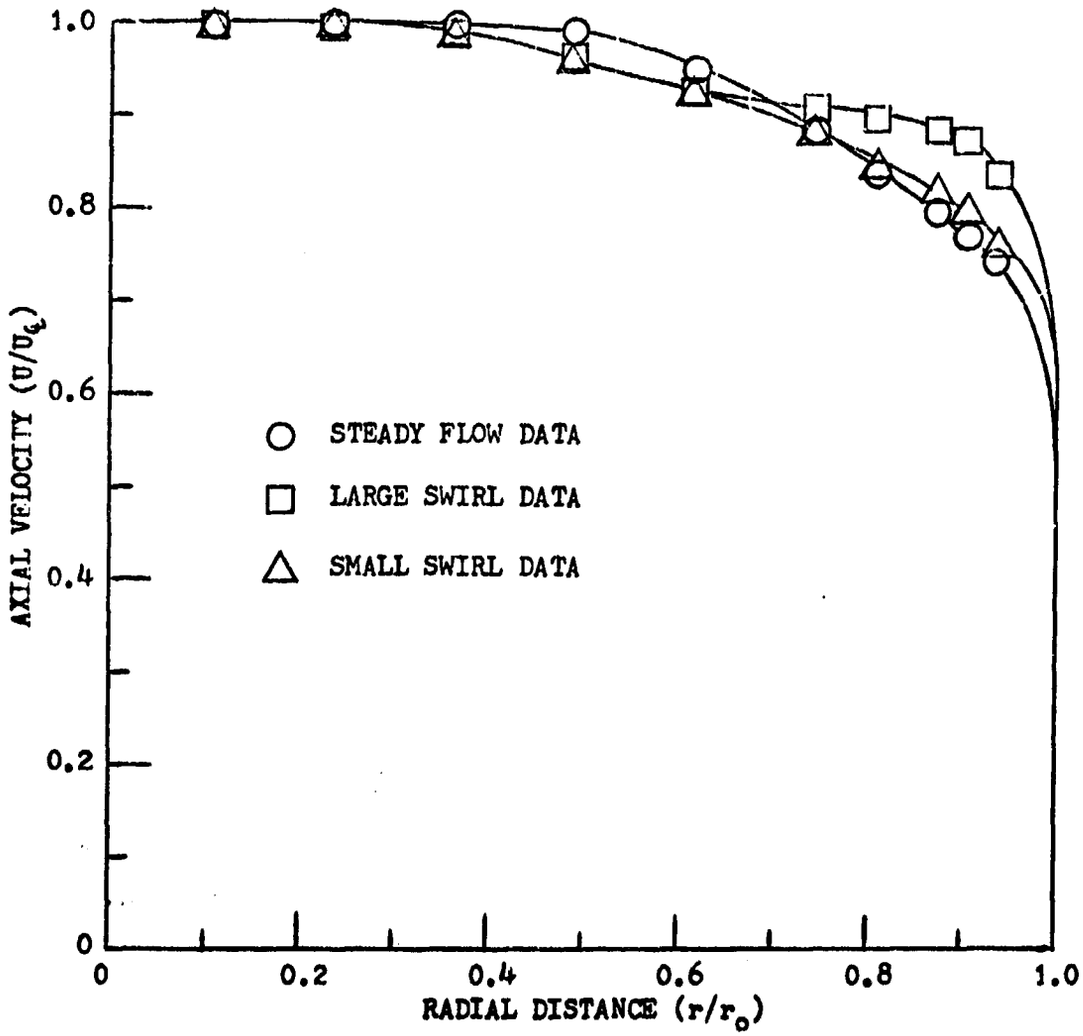

FIGURE 11. RADIAL DISTRIBUTION OF AXIAL VELOCITY AT STATION #2 FOR STEADY AND SWIRLING FLOW

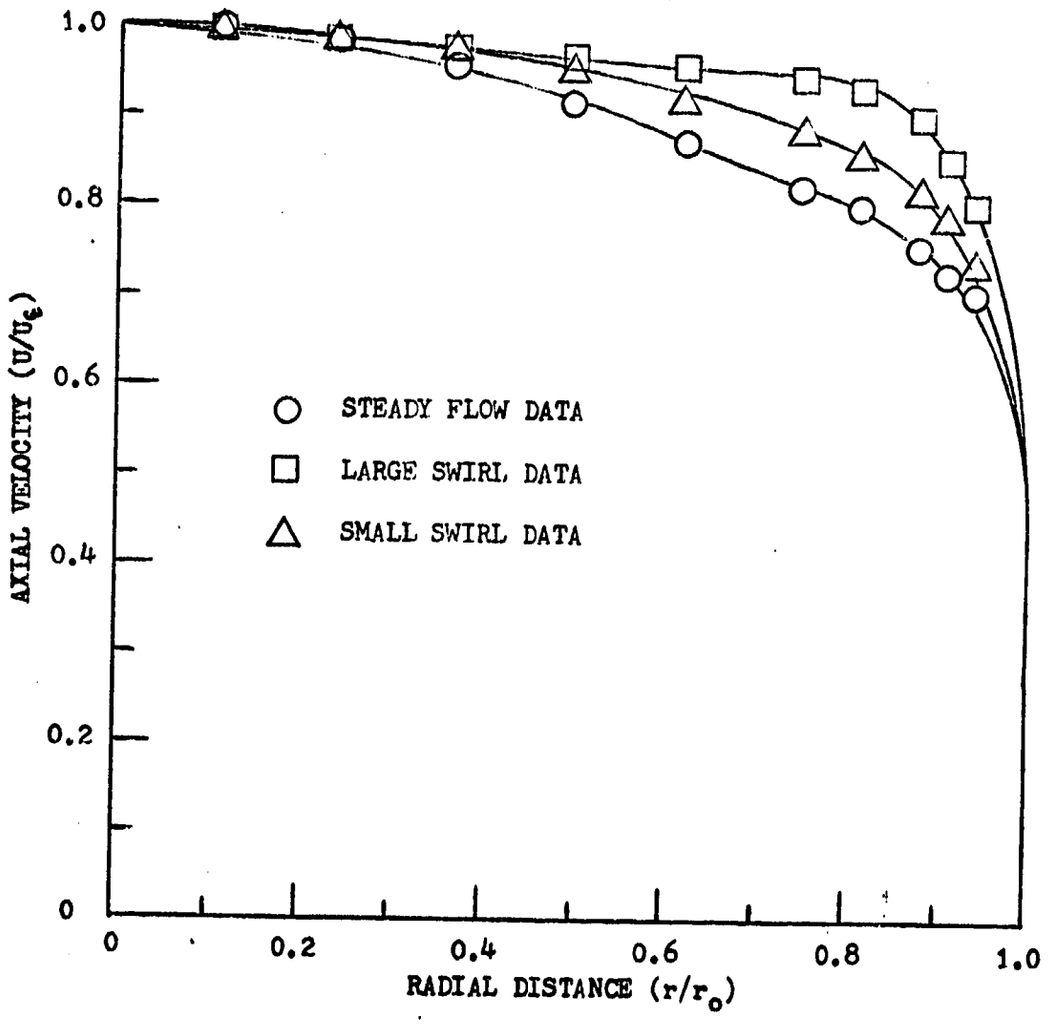

FIGURE 12. RADIAL DISTRIBUTION OF AXIAL VELOCITY AT STATION #3 FOR STEADY AND SWIRLING FLOW

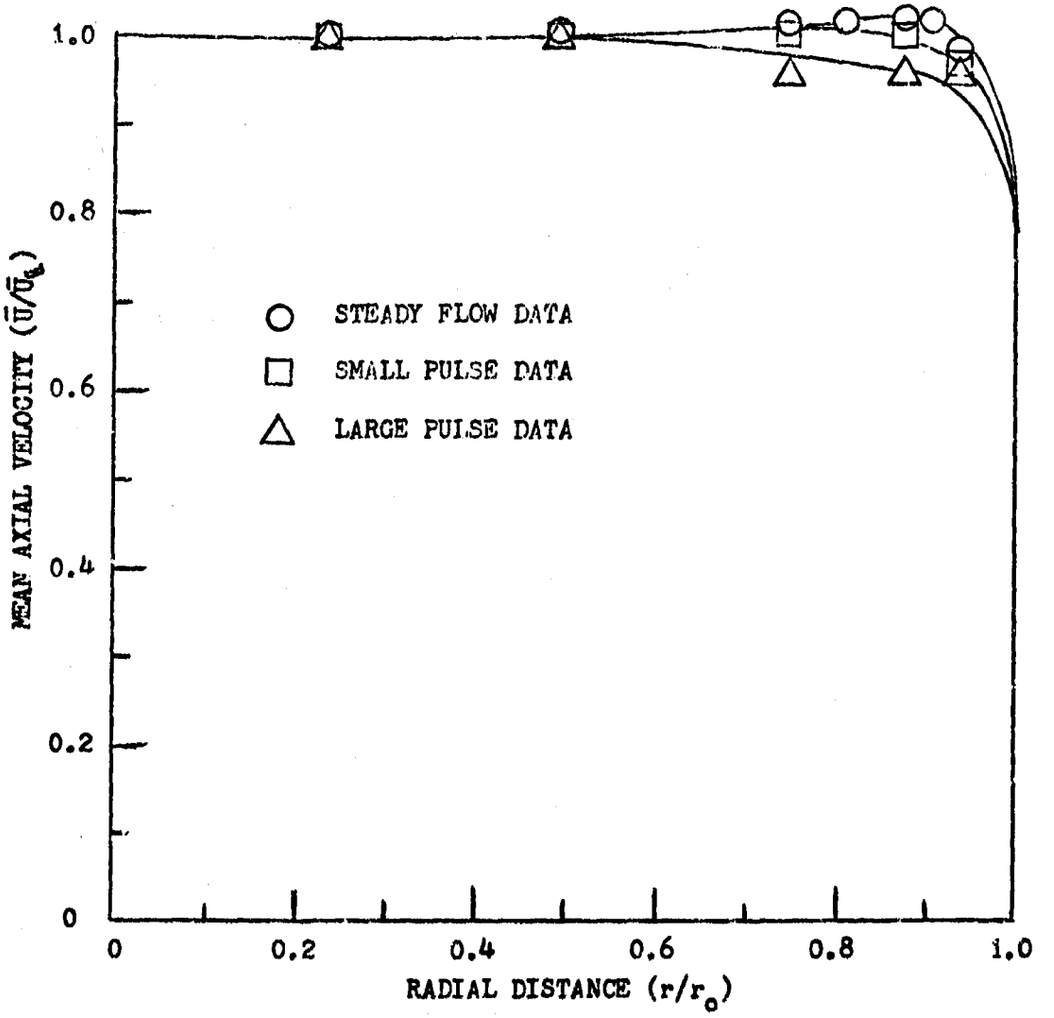

FIGURE 13. RADIAL DISTRIBUTION OF MEAN AXIAL VELOCITY AT STATION #1 FOR STEADY AND PULSING FLOW

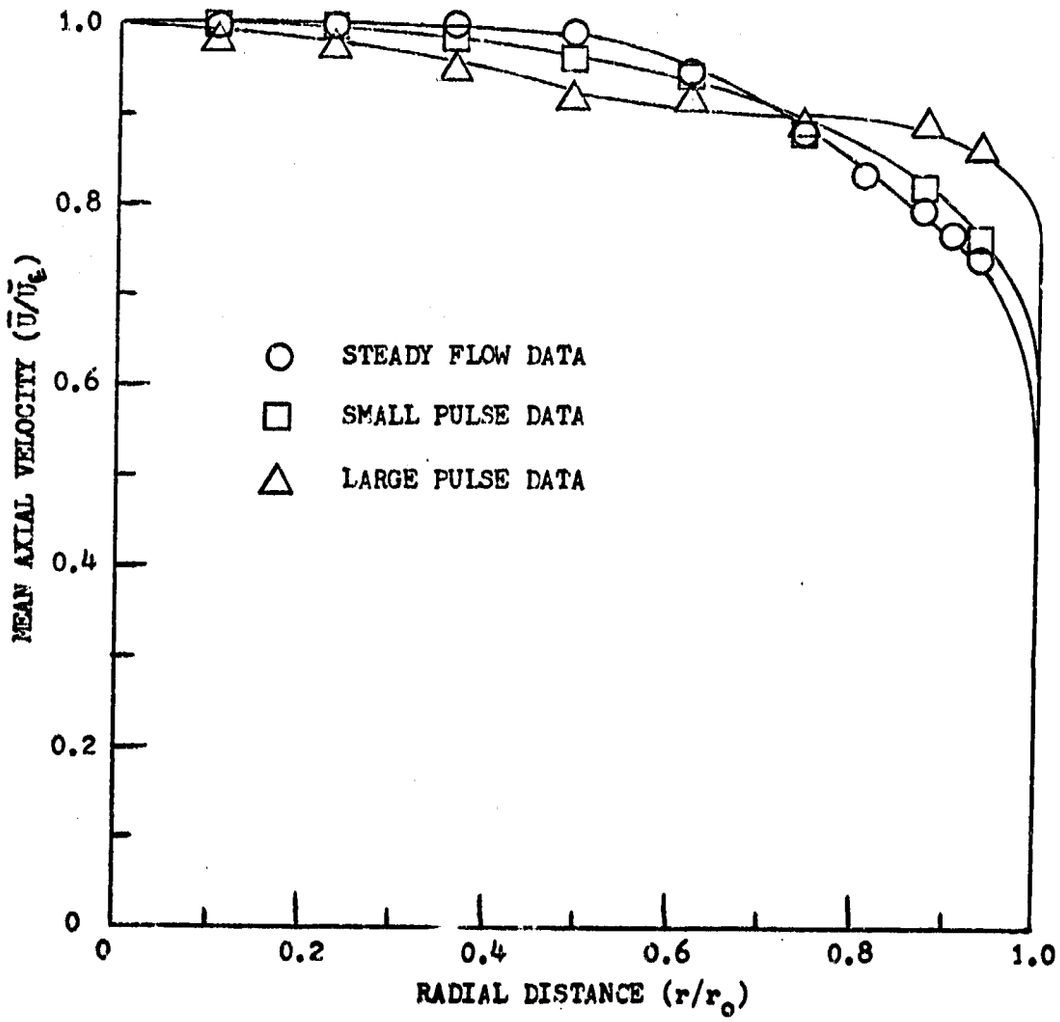

FIGURE 14. RADIAL DISTRIBUTION OF MEAN AXIAL VELOCITY AT STATION #2 FOR STEADY AND PULSING FLOW

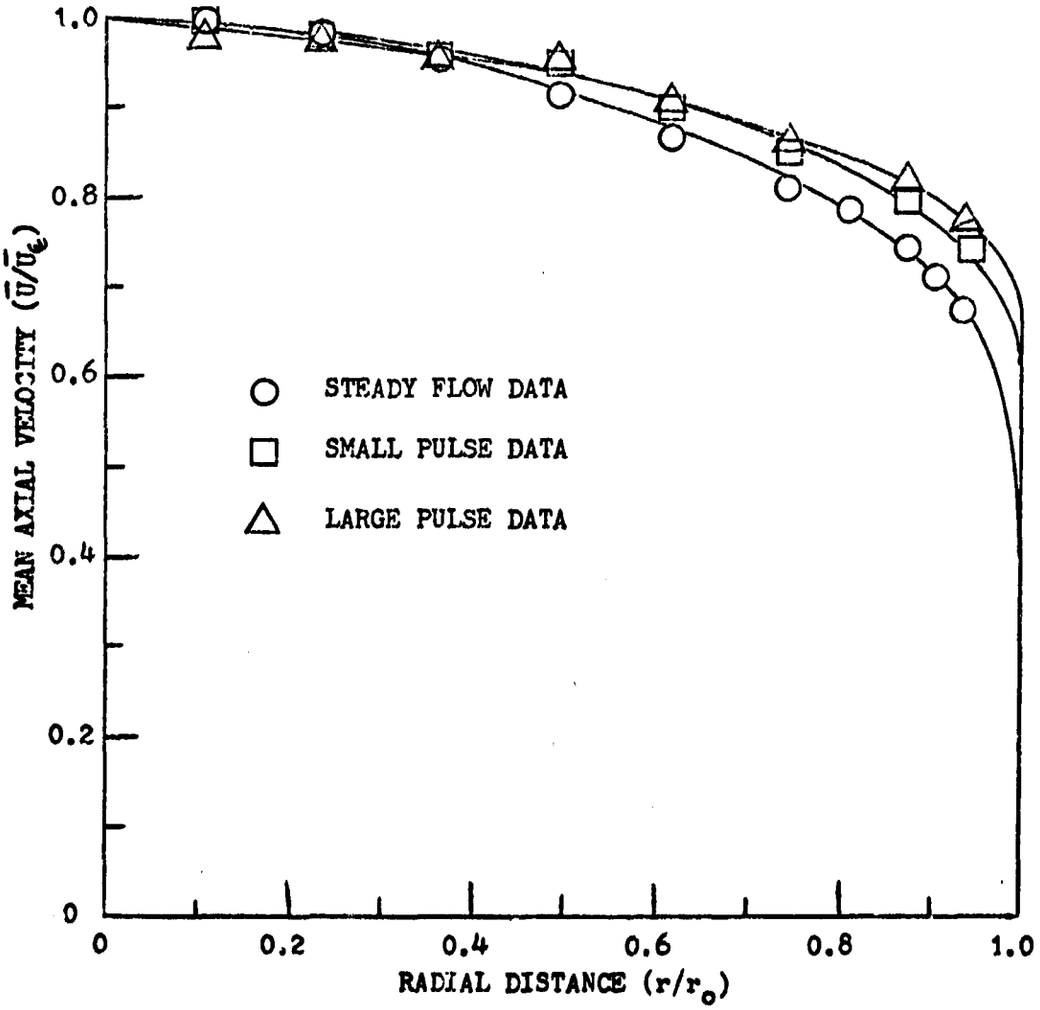

FIGURE 15. RADIAL DISTRIBUTION OF MEAN AXIAL VELOCITY AT STATION #3 FOR STEADY AND PULSING FLOW

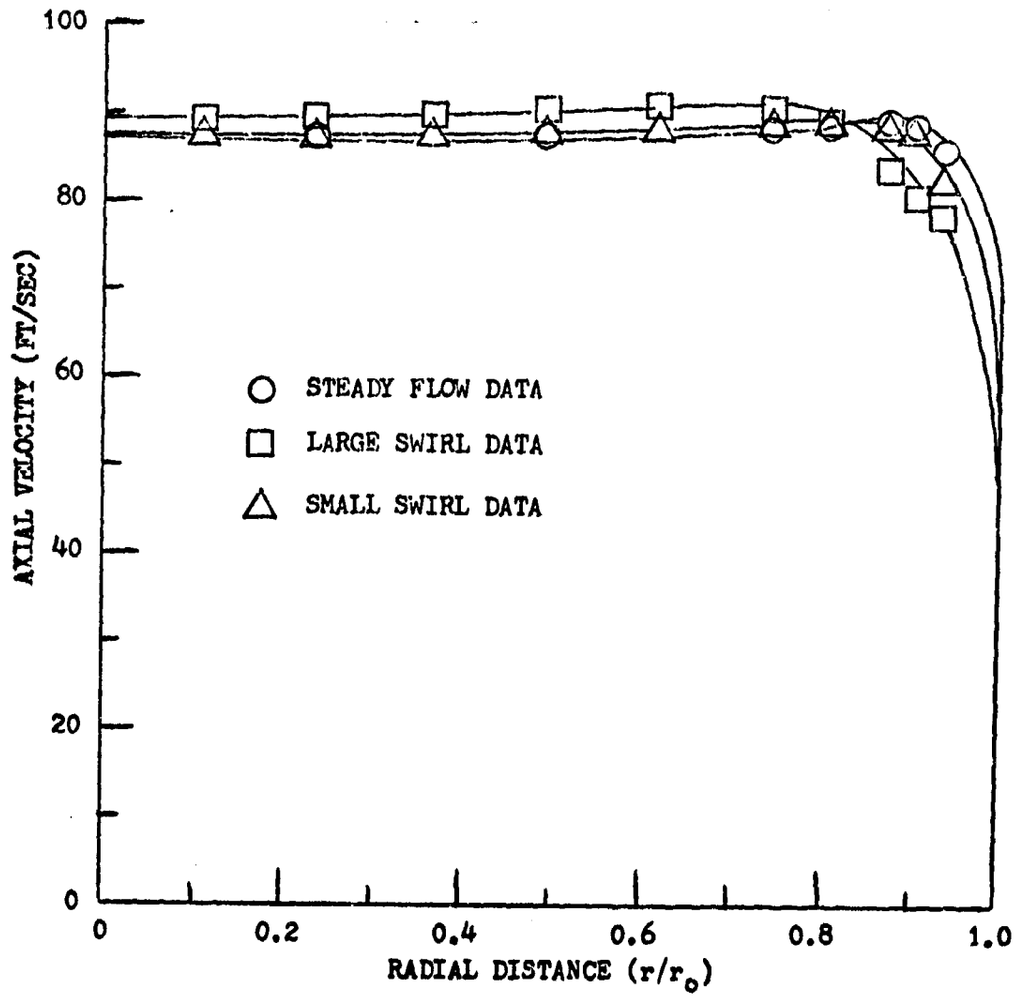

FIGURE 16. RADIAL DISTRIBUTION OF AXIAL VELOCITY AT STATION #1 FOR STEADY AND SWIRLING FLOW

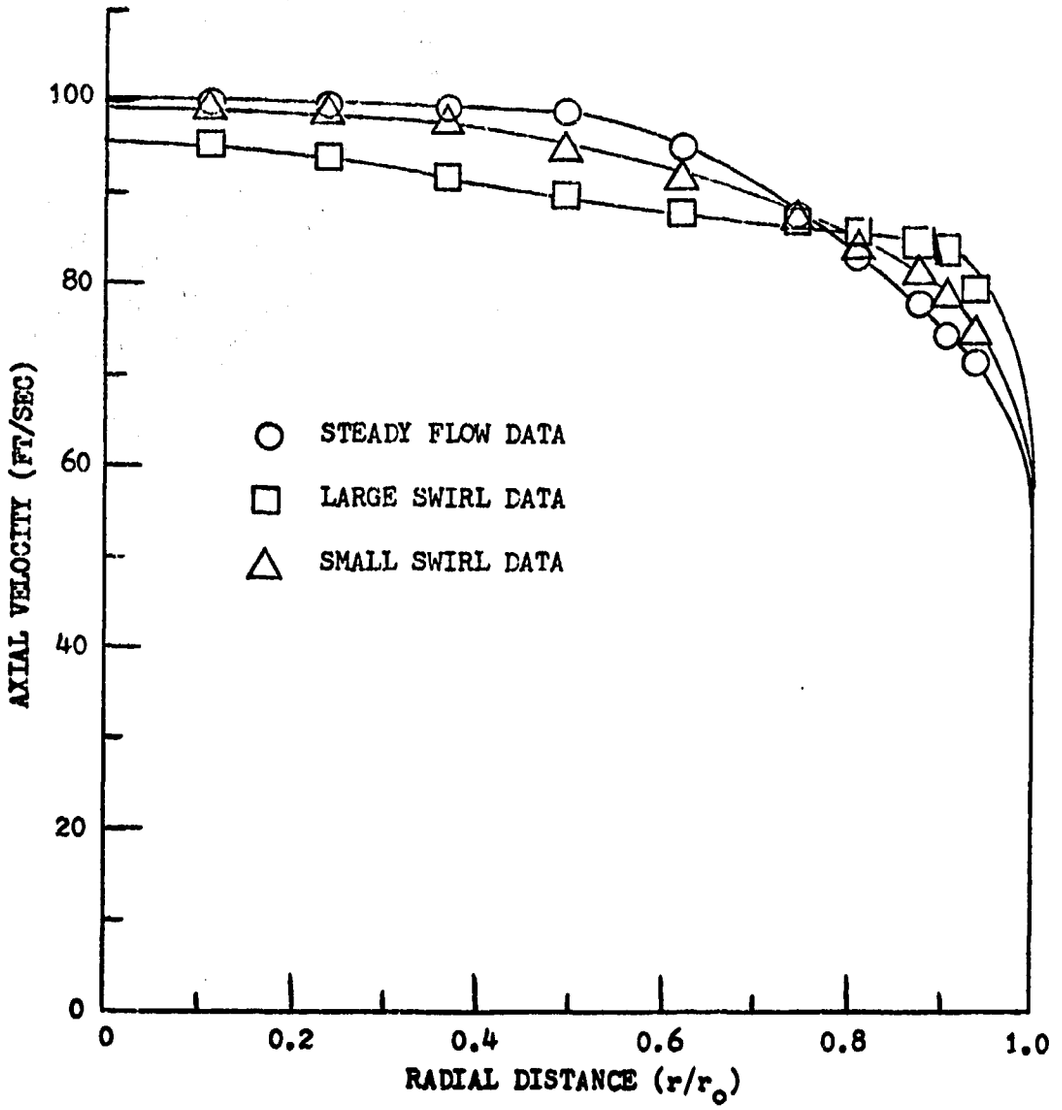

FIGURE 17. RADIAL DISTRIBUTION OF AXIAL VELOCITY AT STATION #2 FOR STEADY AND SWIRLING FLOW

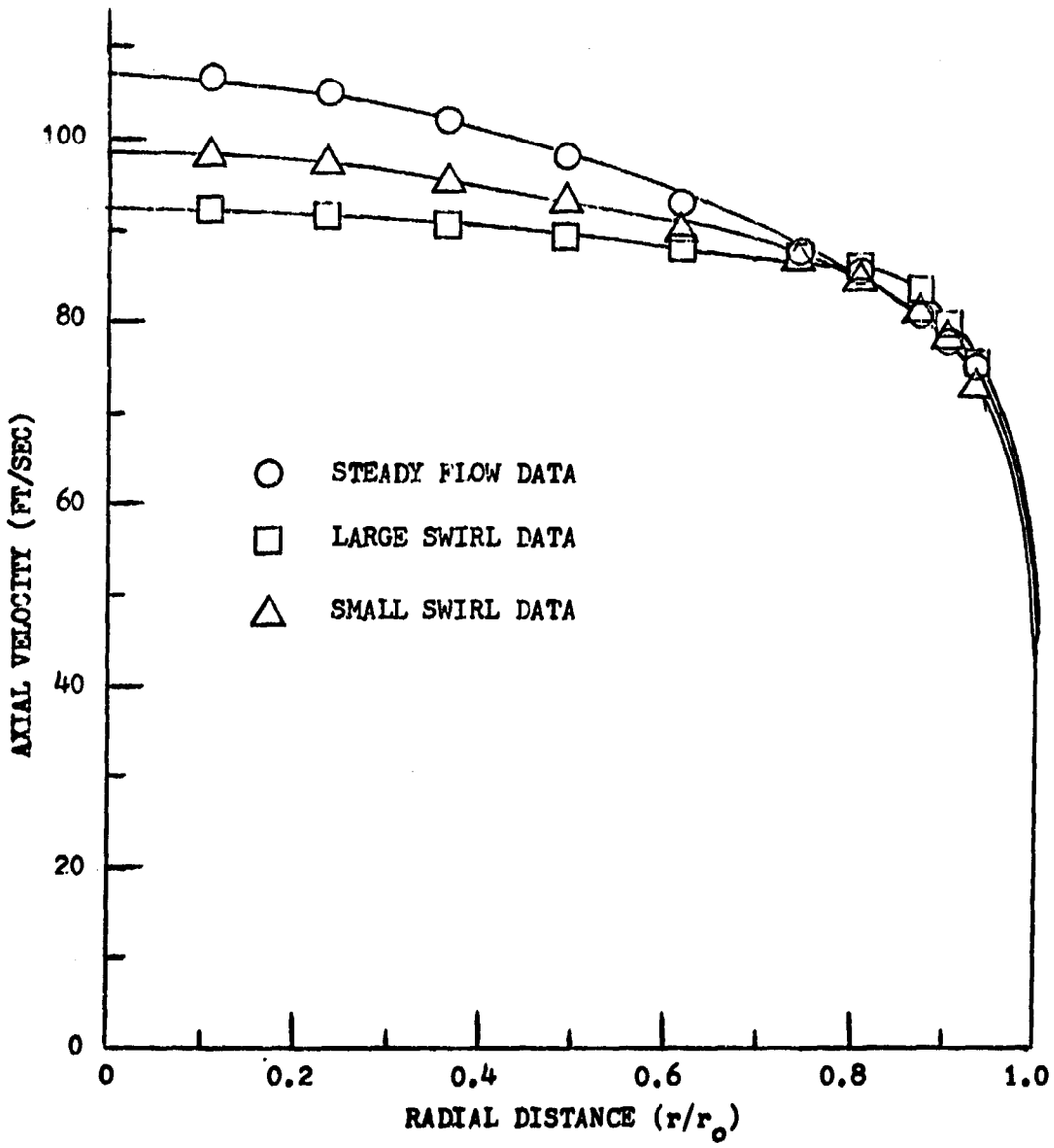

FIGURE 18. RADIAL DISTRIBUTION OF AXIAL VELOCITY AT STATION #3 FOR STEADY AND SWIRLING FLOW

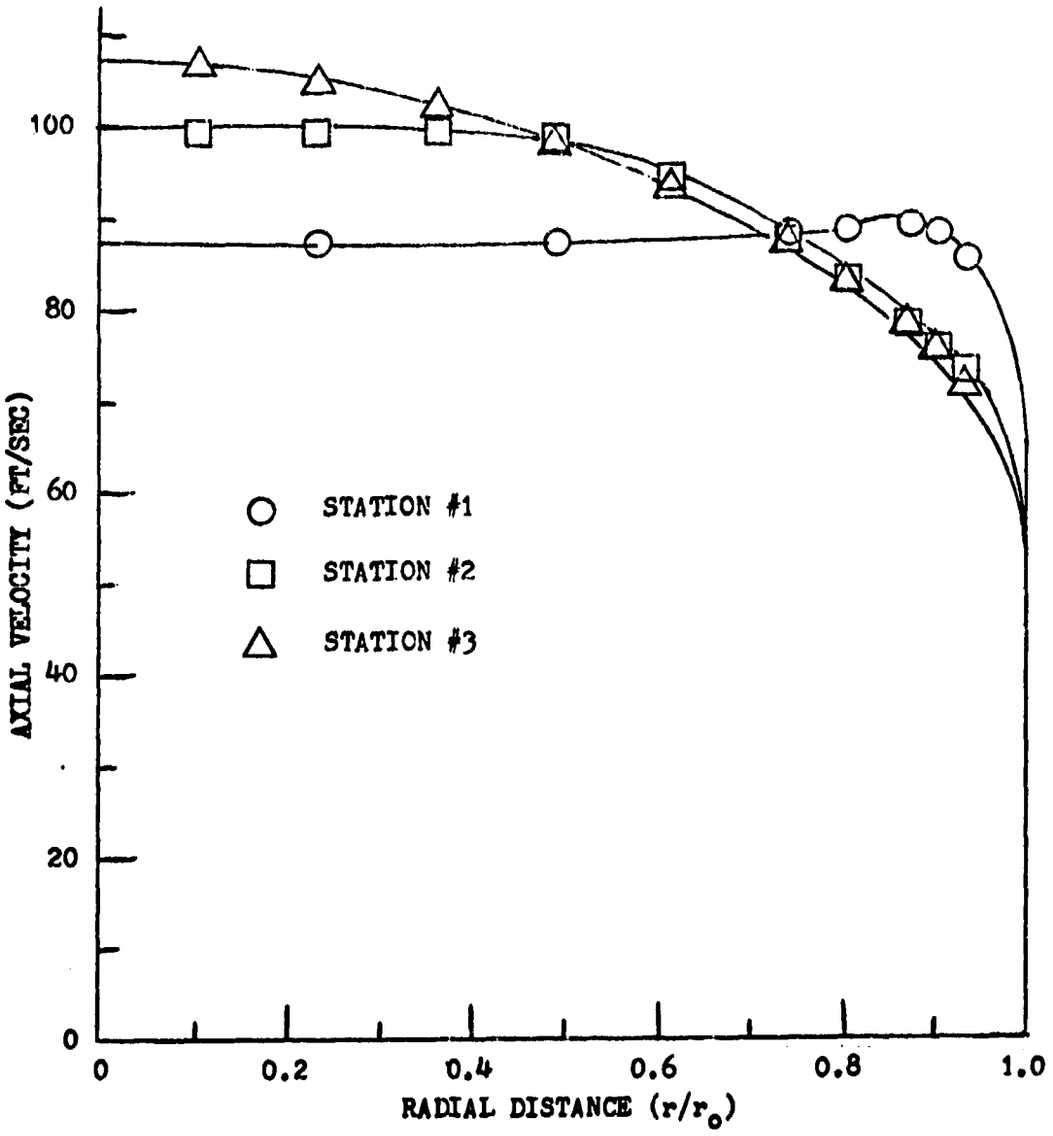

FIGURE 19. COMPARISON OF RADIAL DISTRIBUTION OF AXIAL VELOCITY FOR STEADY FLOW AT STATIONS #1, #2 & #3

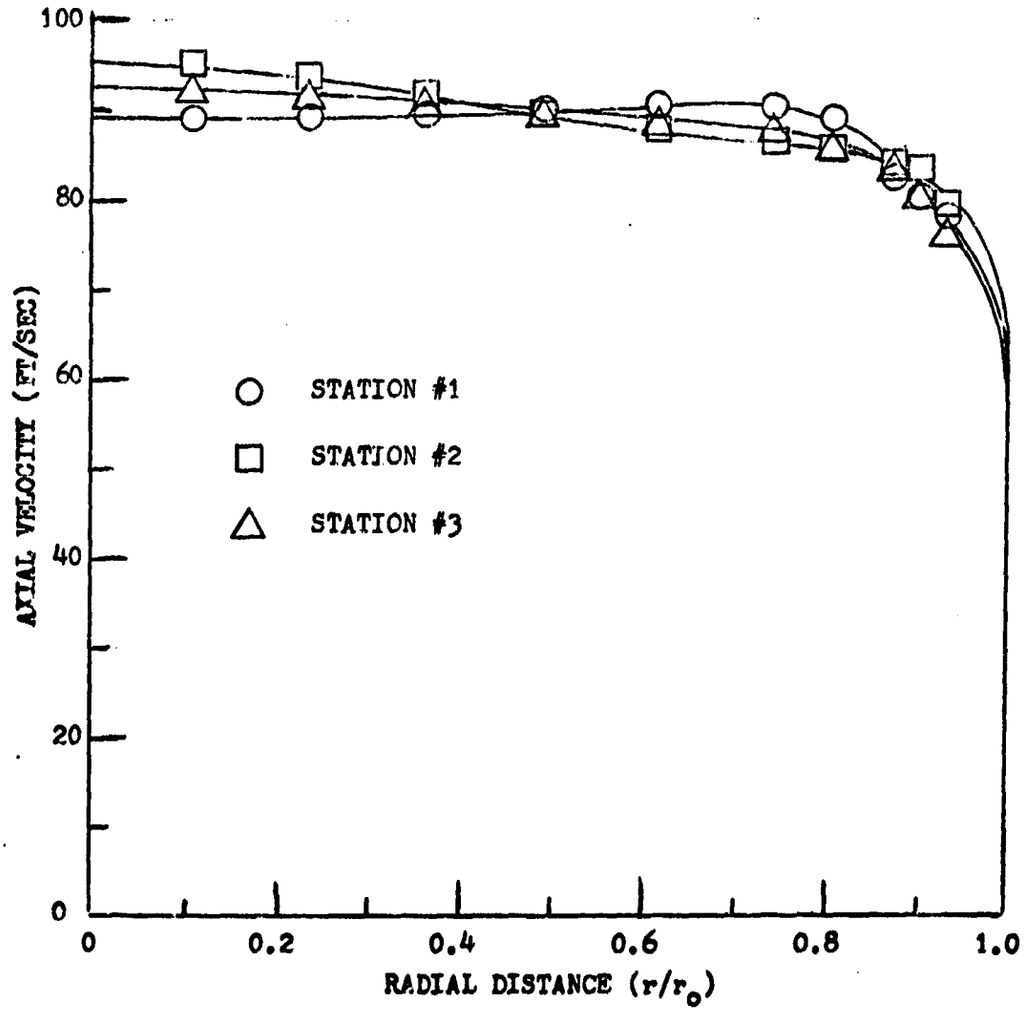

FIGURE 20. COMPARISON OF RADIAL DISTRIBUTION OF AXIAL VELOCITY FOR FLOW WITH LARGE SWIRL AT STATIONS #1, #2 & #3

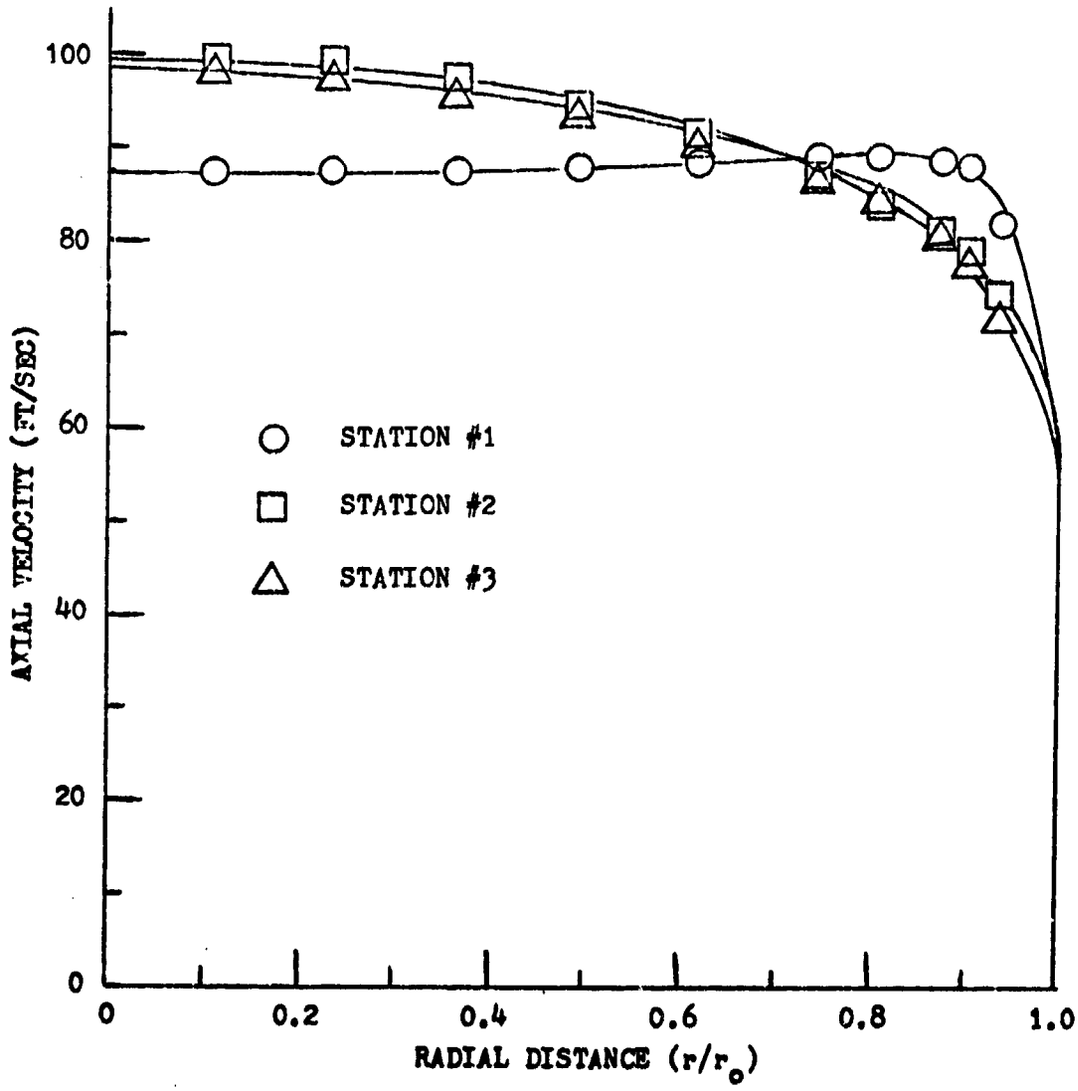

FIGURE 21. COMPARISON OF RADIAL DISTRIBUTION OF AXIAL VELOCITY FOR FLOW WITH SMALL SWIRL AT STATIONS #1, #2 & #3

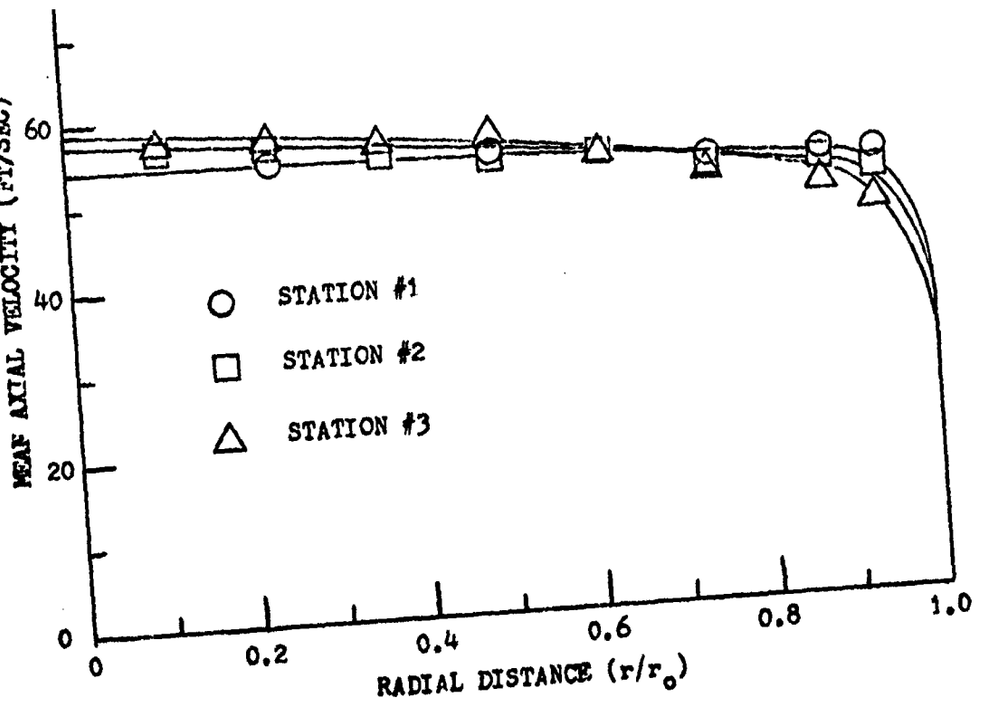

FIGURE 22. COMPARISON OF RADIAL DISTRIBUTION OF MEAN AXIAL VELOCITY FOR FLOW WITH LARGE AMPLITUDE PULSE AT STATIONS #1,#2 & #3

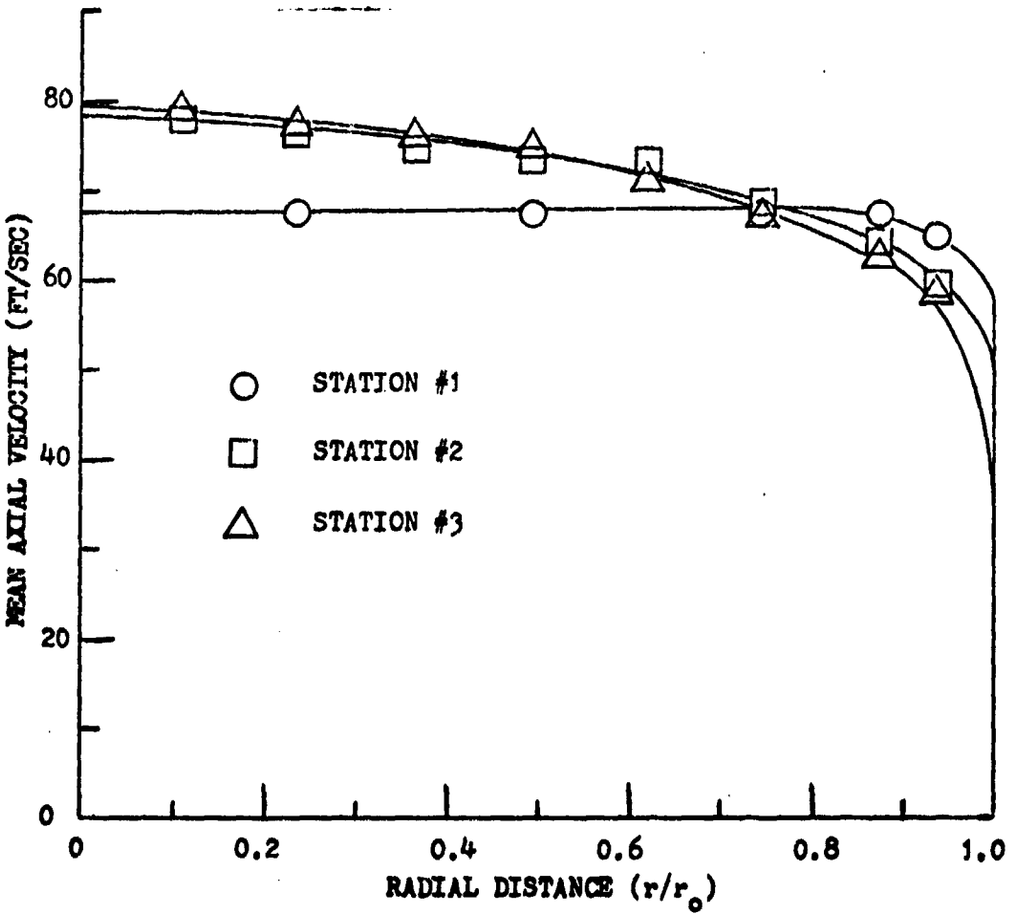

FIGURE 23. COMPARISON OF RADIAL DISTRIBUTION OF MEAN AXIAL VELOCITY FOR FLOW WITH SMALL AMPLITUDE PULSE AT STATIONS #1, #2 & #3

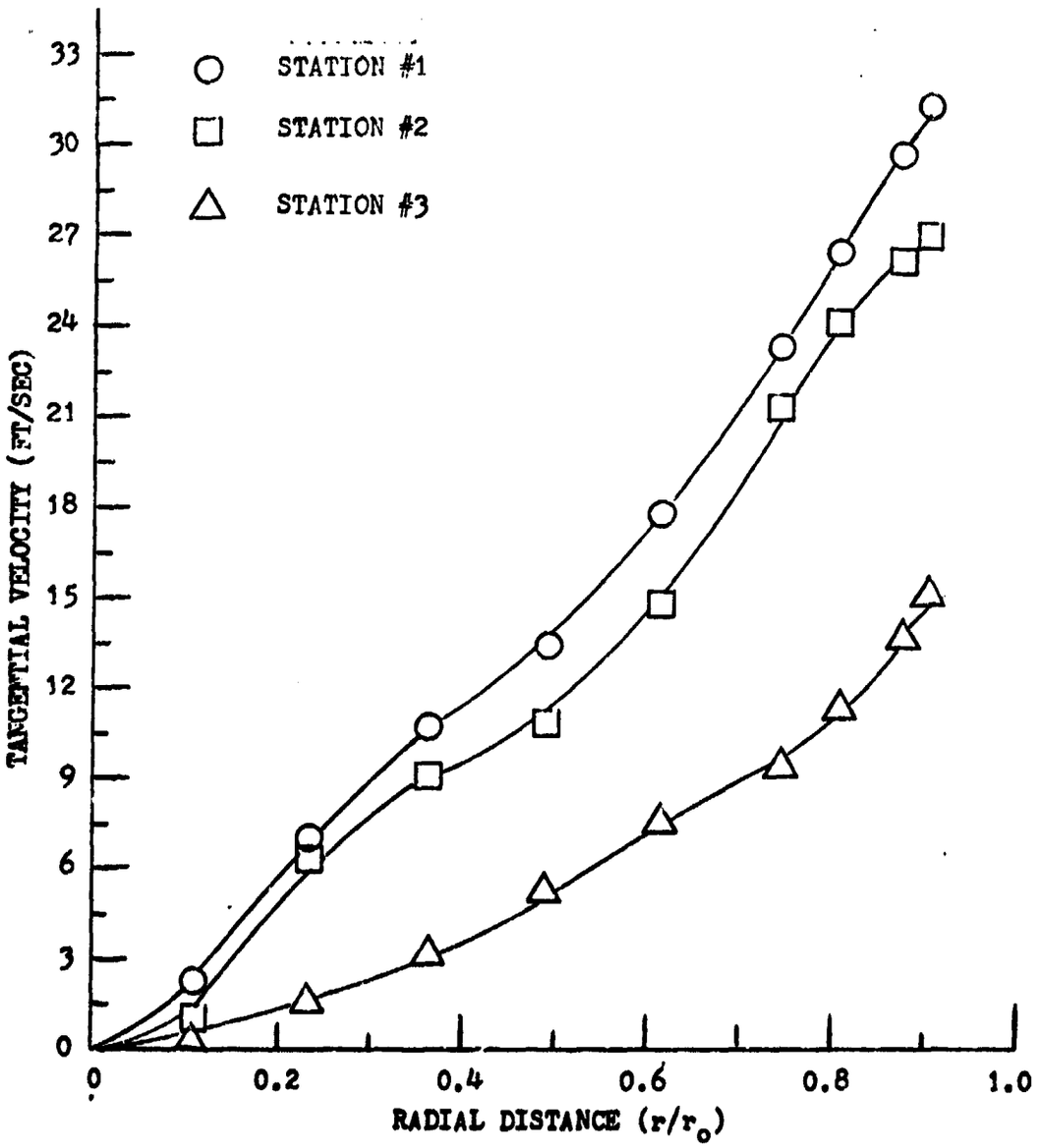

FIGURE 24. COMPARISON OF RADIAL DISTRIBUTION OF TANGENTIAL VELOCITY FOR FLOW WITH LARGE SWIRL AT STATIONS #1, #2 AND #3

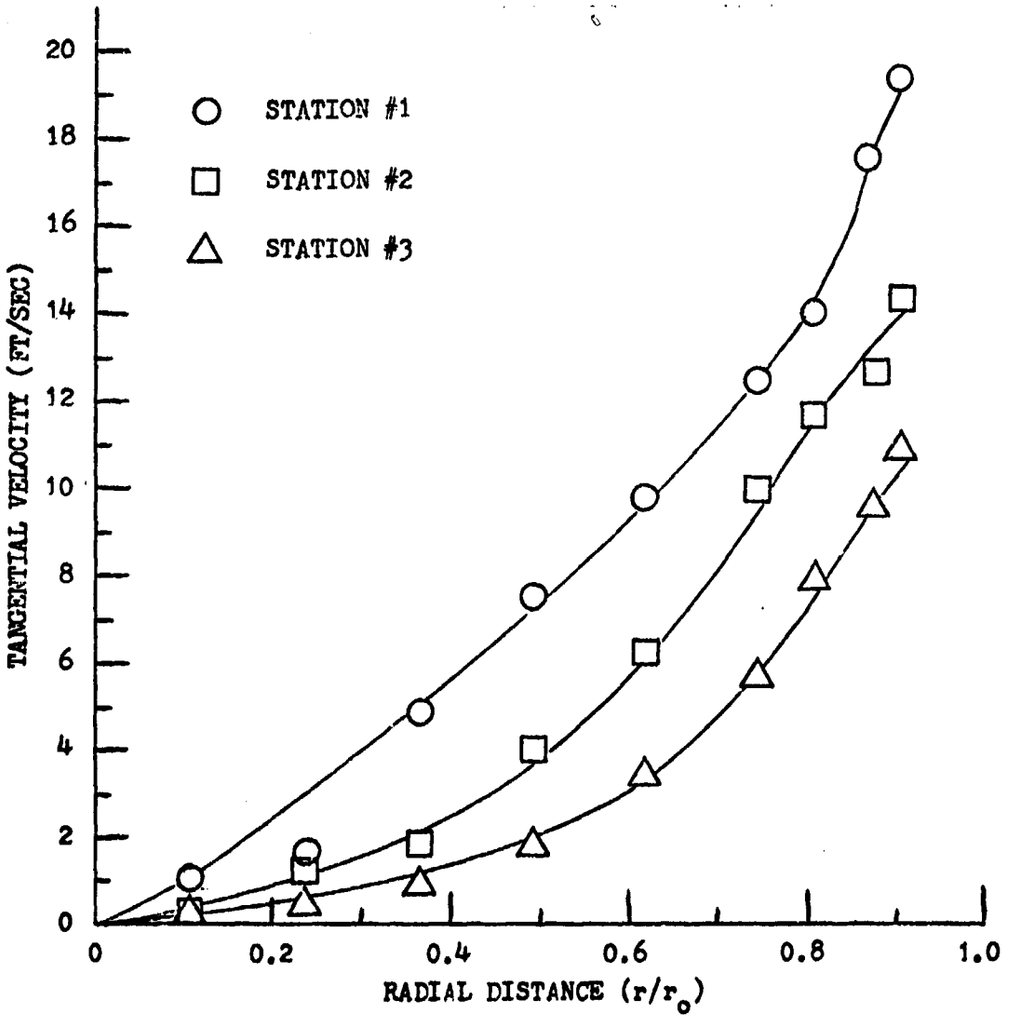

FIGURE 25. COMPARISON OF RADIAL DISTRIBUTION OF TANGENTIAL VELOCITY FOR FLOW WITH SMALL SWIRL AT STATIONS #1, #2 AND #3

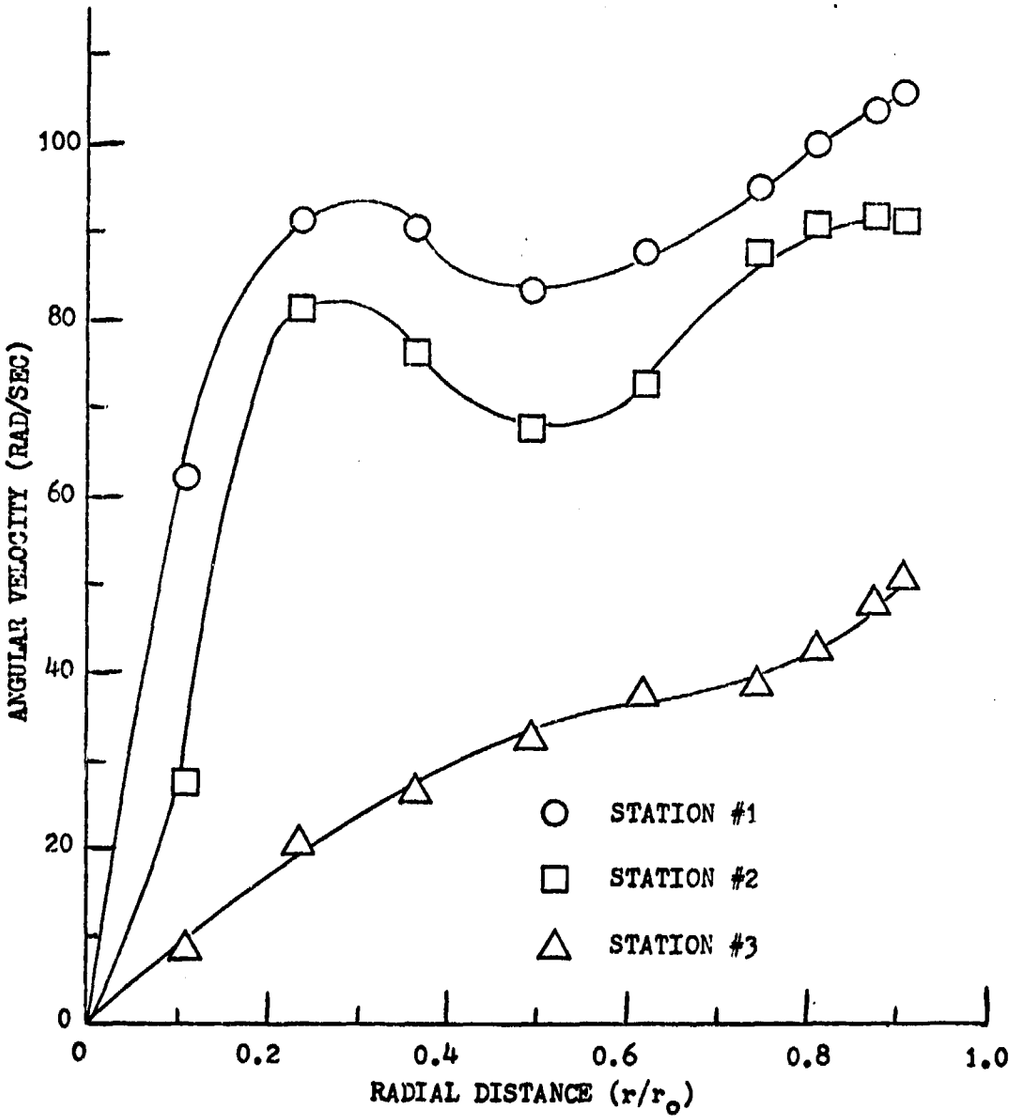

FIGURE 26. COMPARISON OF RADIAL DISTRIBUTION OF ANGULAR VELOCITY FOR FLOW WITH LARGE SWIRL AT STATIONS #1, #2 AND #3

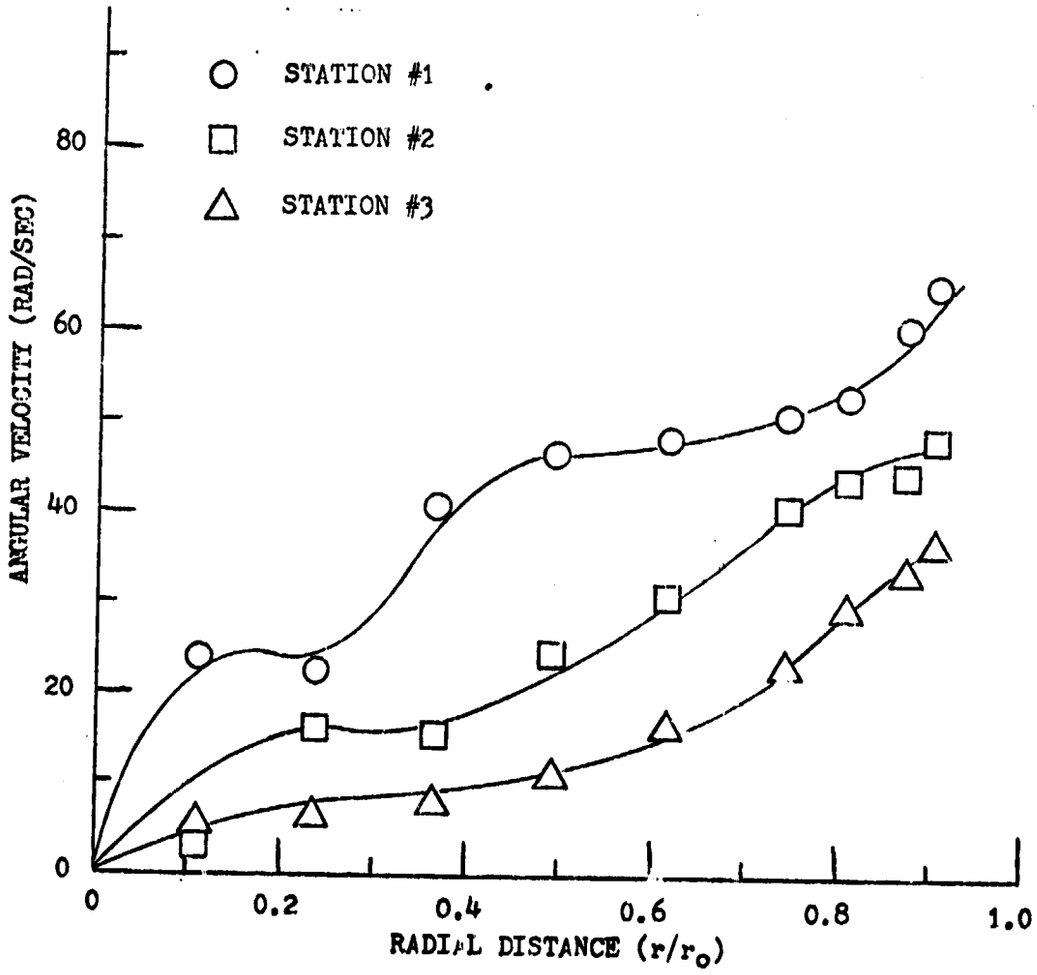

FIGURE 27. COMPARISON OF RADIAL DISTRIBUTION OF ANGULAR VELOCITY FOR FLOW WITH SMALL SWIRL AT STATIONS #1, #2 AND #3

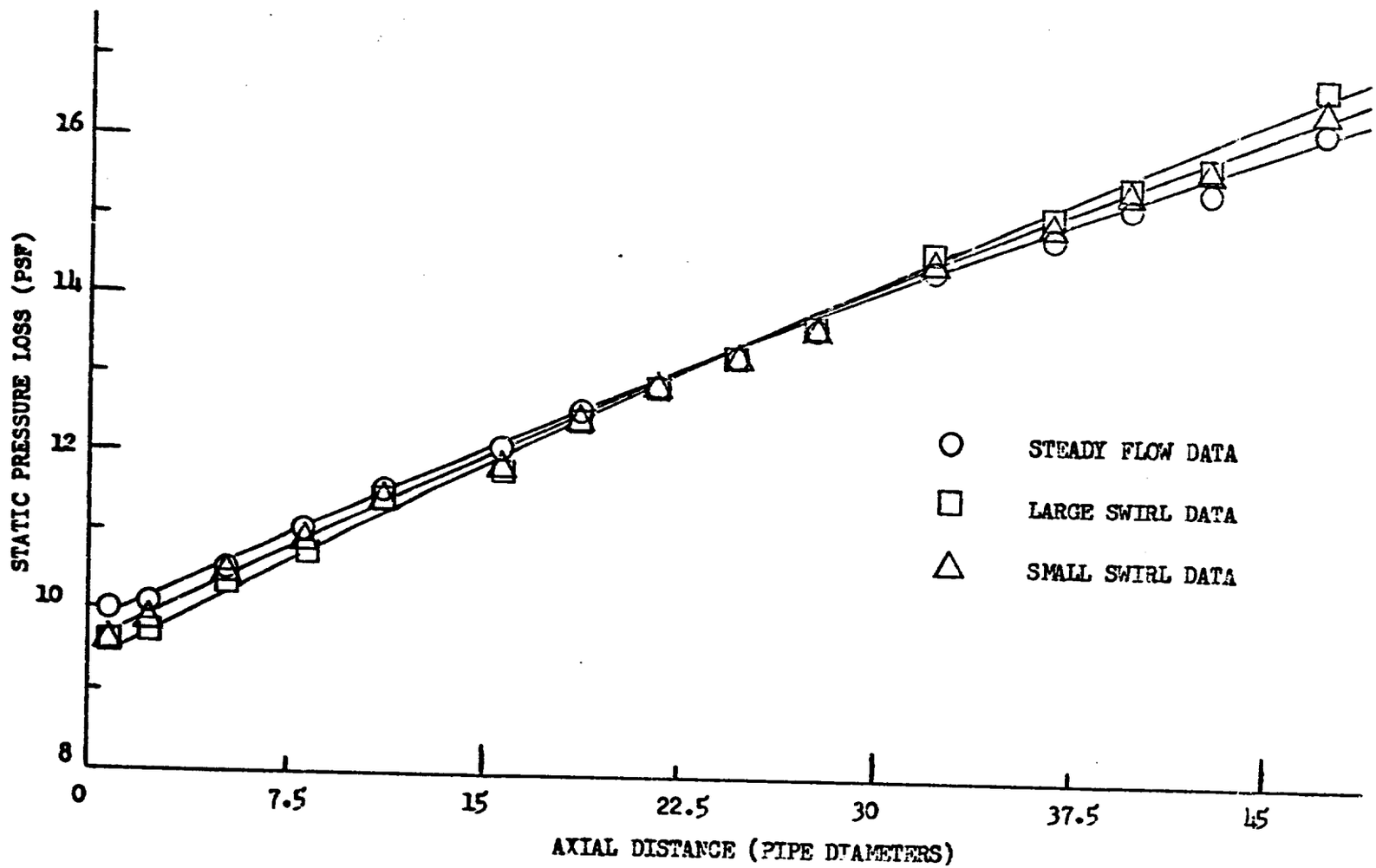

FIGURE 28. AXIAL DISTRIBUTION OF STATIC PRESSURE LOSS FOR STEADY AND SWIRLING FLOW

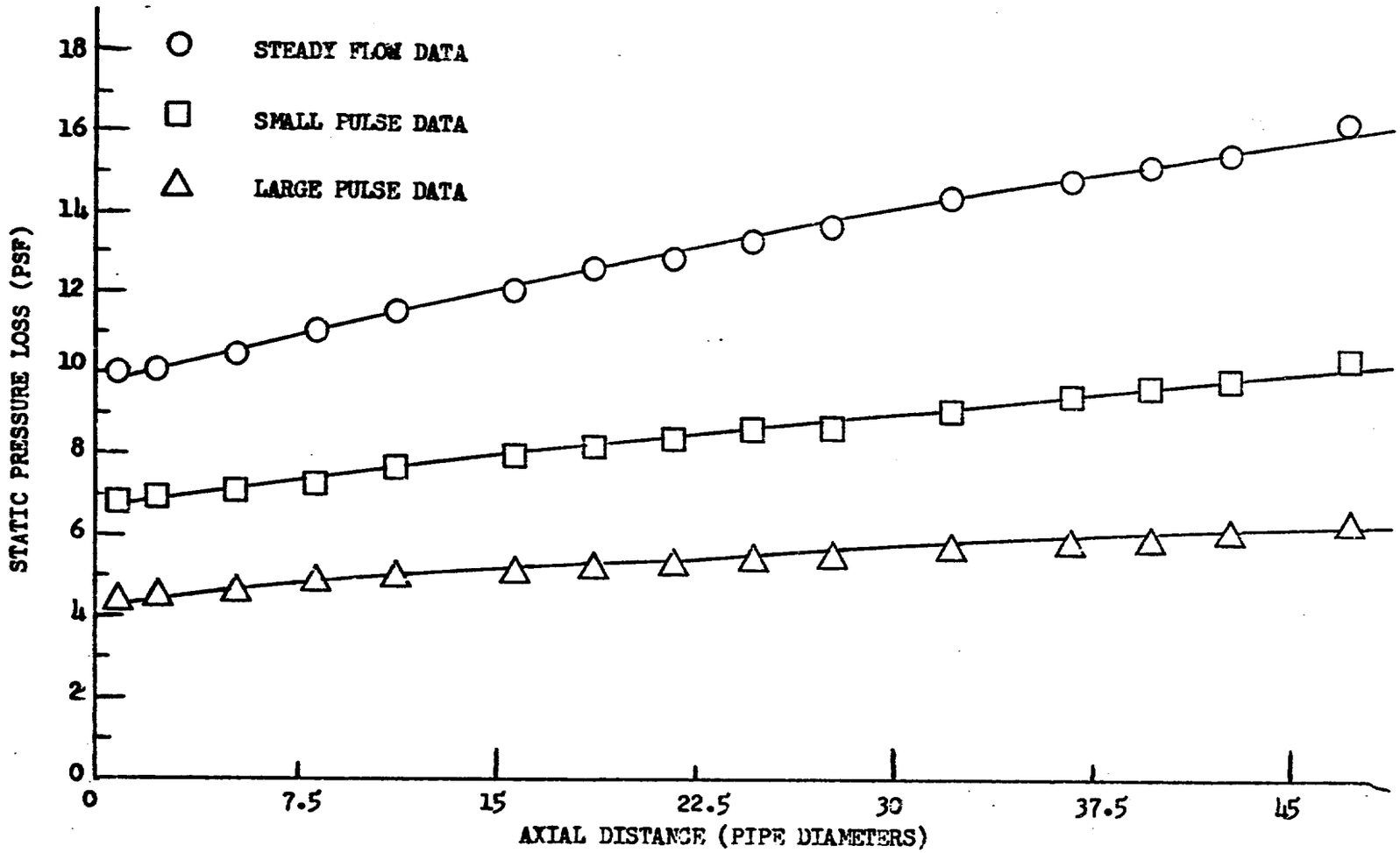

FIGURE 29. AXIAL DISTRIBUTION OF STATIC PRESSURE LOSS FOR STEADY AND PULSING FLOW

APPENDIX A

CALCULATIONS WITH THE X-ARRAY HOT-WIRE ANEMOMETER

The hot-wire anemometer, in essence, consists of a fine electrically heated tungsten wire (4×10^{-4} in. in diameter) which is convectively cooled when placed in an airstream. The resistance of the wire, which varies with its temperature, is related to the mean speed of the airstream and the wire heating current. Thus, the measurement of the voltage drop across the wire relates to the mean velocity of the flow.

The X-array hot-wires (Fig. 8) are separated by an angle of 90° and are inclined at an angle of 45° to the undisturbed flow. With the X-array hot-wire probes connected to the anemometer and the corresponding linearized output fed into the correlator (see Fig. 9), voltage readings can be made for E_a, E_b, E_a+E_b, and E_a-E_b. (E_a and E_b refer to the voltage drop across wire a and wire b respectively).

Since the hot-wire responds to flow normal to it, by simple trigonometry,

$$E_a = C_a(U + V_\theta) \qquad (1)$$

$$E_b = C_b(U - V_\theta) \qquad (2)$$

When $V_\theta = 0$ (no swirl), E_a is set equal to E_b so that $C_a = C_b = C$. By use of the pitot static tube, the local velocity in the duct can be obtained and used to calibrate the hot-wire probes. Now, with $V_\theta = 0$ and $C_a = C_b = C$, equations (1) and (2) give,

$$U = \frac{1}{2C}(E_a + E_b) \qquad (3)$$

$$V_\theta = \frac{1}{2C}(E_a - E_b) \qquad (4)$$

Since the voltage output of the anemometer is linearized, equations (3) and (4) are used to determine the U and V_θ velocities from the voltage readings obtained at the various stations in the duct.

APPENDIX B

STEADY FLOW DATA

Station #1

r/r_o	Raw Data Pitot (in. H_2O)	Raw Data Hot-wire (volts)	Pitot U (ft/sec)	Pitot U/U_{ℓ}	Hot-wire U (ft/sec)	Hot-wire U/U_{ℓ}
0.937	3.33	4.90	86.52	0.991	85.54	0.980
0.905	3.47	5.12	88.32	1.012	89.32	1.024
0.873	3.52	5.13	88.95	1.019	89.56	1.026
0.810	3.50	5.115	88.70	1.016	89.30	1.023
0.746	3.48	5.105	88.45	1.013	89.12	1.021
0.492	3.42	5.035	87.68	1.004	87.90	1.007
0.238	3.40	5.03	87.42	1.001	87.81	1.006
0.00	3.39	5.00	87.29	1.00	87.29	1.00

Station #2

r/r_o	Raw Data Pitot (in. H_2O)	Raw Data Hot-wire (volts)	Pitot U (ft/sec)	Pitot U/U_{ℓ}	Hot-wire U (ft/sec)	Hot-wire U/U_{ℓ}
0.937	2.46	5.60	74.36	0.743	70.01	0.700
0.905	2.63	5.89	76.89	0.769	73.64	0.730
0.873	2.82	6.145	79.62	0.796	76.83	0.768
0.810	3.09	6.64	83.34	0.833	83.02	0.830
0.746	3.44	7.005	87.94	0.879	87.58	0.876
0.619	4.00	7.615	94.82	0.948	95.21	0.952
0.492	4.36	7.945	94.00	0.990	99.33	0.993
0.365	4.43	7.985	99.79	0.998	99.83	0.998
0.238	4.44	7.995	99.90	0.999	99.96	0.999
0.111	4.44	8.00	99.90	0.999	100.02	1.00
0.00	4.45	8.00	100.02	1.00	100.02	1.00

Station #3

r/r_o	Raw Data Pitot (in. H_2O)	Raw Data Hot-wire (volts)	Pitot U (ft/sec)	Pitot U/U_ℓ	Hot-wire U (ft/sec)	Hot-wire U/U_ℓ
0.937	2.52	6.63	75.27	0.702	71.06	0.663
0.905	2.70	7.09	77.91	0.727	75.99	0.709
0.873	2.90	7.36	80.75	0.753	78.88	0.736
0.810	3.28	7.78	85.87	0.801	83.39	0.778
0.746	3.45	9.095	88.07	0.822	86.76	0.809
0.619	3.88	8.665	93.40	0.871	92.87	0.866
0.492	4.29	9.11	98.21	0.916	97.64	0.911
0.365	4.67	9.48	102.47	0.956	101.61	0.948
0.238	4.96	9.81	105.60	0.985	105.14	0.981
0.111	5.10	9.975	107.08	0.999	106.91	0.997
0.00	5.11	10.00	107.18	1.00	107.18	1.00

APPENDIX C

SWIRLING FLOW DATA

Station #1

Large Swirl

r/r_o	Raw Data U (volts)	Raw Data V_θ (volts)	U (ft/sec)	U/U_∞	V_θ (ft/sec)	W (rad/sec)
0.937	4.48	---	78.21	0.878	---	---
0.905	4.60	1.80	80.31	0.901	31.42	105.84
0.873	4.79	1.70	83.62	0.938	29.68	103.61
0.810	5.10	1.52	89.04	0.999	26.54	99.92
0.746	5.18	1.33	90.43	1.015	23.22	94.86
0.619	5.19	1.02	90.61	1.017	17.81	87.69
0.492	5.17	0.77	90.26	1.013	13.44	83.24
0.365	5.15	0.62	89.90	1.009	10.82	90.34
0.238	5.13	0.41	89.56	1.005	7.16	91.65
0.111	5.12	0.13	89.38	1.003	2.27	62.32
0.00	5.105	0.0	89.12	1.00	0.00	0.00

Station #1

Small Swirl

r/r_o	Raw Data U (volts)	Raw Data V_θ (volts)	U (ft/sec)	U/U_∞	V_θ (ft/sec)	W (rad/sec)
0.937	4.70	---	82.05	0.937	---	---
0.905	5.06	1.11	88.34	1.009	19.38	65.28
0.873	5.10	1.00	89.04	1.017	17.46	60.95
0.810	5.11	0.80	89.21	1.019	13.97	52.59
0.746	5.105	0.71	89.12	1.018	12.40	50.66
0.619	5.08	0.56	88.66	1.013	9.77	48.10
0.492	5.045	0.43	88.08	1.006	7.51	46.51
0.365	5.035	0.28	87.87	1.004	4.88	40.75
0.238	5.015	0.10	87.55	1.00	1.75	22.40
0.111	5.01	0.05	87.43	0.999	0.87	23.89
0.00	5.015	0.00	87.55	1.00	0.00	0.00

Station #2

Large Swirl

r/r_o	Raw Data U (volts)	Raw Data V_θ (volts)	U (ft/sec)	U/U_ℓ	V_θ (ft/sec)	W (rad/sec)
0.937	6.38	---	79.77	0.835	---	---
0.905	6.70	2.16	83.77	0.876	27.01	90.98
0.873	6.755	2.09	84.45	0.884	26.13	91.22
0.810	6.86	1.93	85.77	0.897	24.13	90.84
0.746	6.935	1.71	86.70	0.907	21.38	87.34
0.619	7.04	1.18	88.02	0.921	14.75	72.62
0.492	7.19	0.87	89.89	0.940	10.88	67.39
0.365	7.35	0.73	91.89	0.961	9.13	76.22
0.238	7.515	0.51	93.96	0.983	6.38	81.66
0.111	7.62	0.08	95.27	0.997	1.00	27.43
0.00	7.645	0.00	95.58	1.00	0.00	0.00

Station #2

Small Swirl

r/r_o	Raw Data U (volts)	Raw Data V_θ (volts)	U (ft/sec)	U/U_ℓ	V_θ (ft/sec)	W (rad/sec)
0.937	5.98	---	74.76	0.751	---	---
0.905	6.32	1.15	79.02	0.794	14.38	48.44
0.873	6.51	1.01	81.39	0.817	12.63	44.09
0.810	6.72	0.93	84.02	0.844	11.63	43.78
0.746	6.985	0.80	87.33	0.877	10.00	40.85
0.619	7.335	0.50	91.71	0.921	6.25	30.77
0.492	7.59	0.32	94.89	0.953	4.00	24.77
0.365	7.815	0.15	97.71	0.981	1.88	15.65
0.238	7.935	0.10	99.21	0.996	1.25	16.00
0.111	7.96	0.01	99.52	0.999	0.13	3.43
0.00	7.965	0.00	99.58	1.00	0.00	0.00

Station #3

Large Swirl

r/r_o	Raw Data U (volts)	Raw Data V_θ (volts)	U (ft/sec)	U/U_∞	V_θ (ft/sec)	W (rad/sec)
0.937	7.01	---	75.13	0.810	---	---
0.905	7.38	1.41	79.10	0.853	15.11	50.90
0.873	7.80	1.28	83.60	0.901	13.72	47.90
0.810	8.055	1.06	86.33	0.931	11.36	42.77
0.746	8.135	0.88	87.19	0.940	9.43	38.52
0.619	8.24	0.71	88.32	0.952	7.61	37.46
0.492	8.36	0.49	89.60	0.966	5.25	32.52
0.365	8.435	0.30	90.41	0.975	3.22	26.88
0.238	8.54	0.15	91.53	0.987	1.61	20.61
0.111	8.61	0.03	92.28	0.995	0.32	8.78
0.00	8.655	0.00	92.76	1.00	0.00	0.00

Station #3

Small Swirl

r/r_o	Raw Data U (volts)	Raw Data V_θ (volts)	U (ft/sec)	U/U_∞	V_θ (ft/sec)	W (rad/sec)
0.937	6.71	---	71.92	0.731	---	---
0.905	7.23	1.02	77.49	0.787	10.93	36.82
0.873	7.515	0.90	80.55	0.818	9.65	33.69
0.810	7.965	0.74	84.30	0.856	7.93	29.85
0.746	8.11	0.53	86.92	0.883	5.68	23.20
0.619	8.415	0.32	90.19	0.916	3.43	16.89
0.492	8.725	0.17	93.51	0.950	1.82	11.27
0.365	8.935	0.09	95.77	0.973	0.96	8.01
0.238	9.075	0.05	97.27	0.988	0.54	6.91
0.111	9.16	0.02	98.18	0.997	0.21	5.76
0.00	9.185	0.00	98.44	1.00	0.00	0.00

APPENDIX D

PULSING FLOW DATA

Axial Velocity Distribution

Small Amplitude Pulse

Station #1

Volts

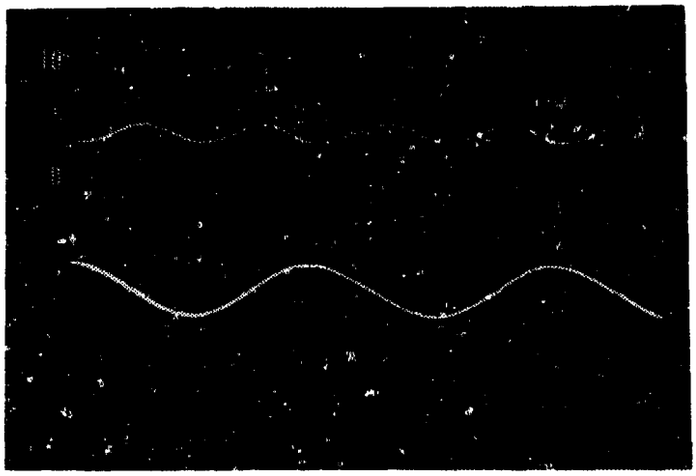

Sweep = 0.5 sec/cm

$r/r_o = 0.00$

Volts

Sweep = 0.5 sec/cm

$r/r_o = 0.238$

Axial Velocity Distribution

Small Amplitude Pulse

Station #1

Volts

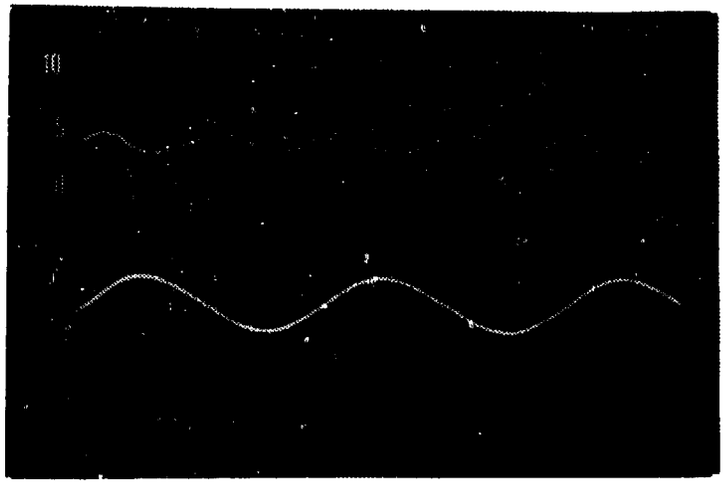

Sweep =
0.5 sec/cm

$r/r_o = 0.462$

volts

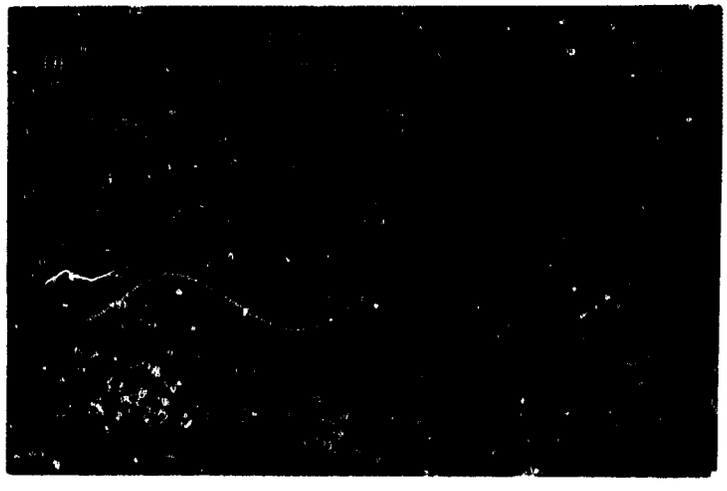

Sweep =
0.5 sec/cm

$r/r_o = 0.746$

Axial Velocity Distribution

Small Amplitude Pulse

Station #1

Volts

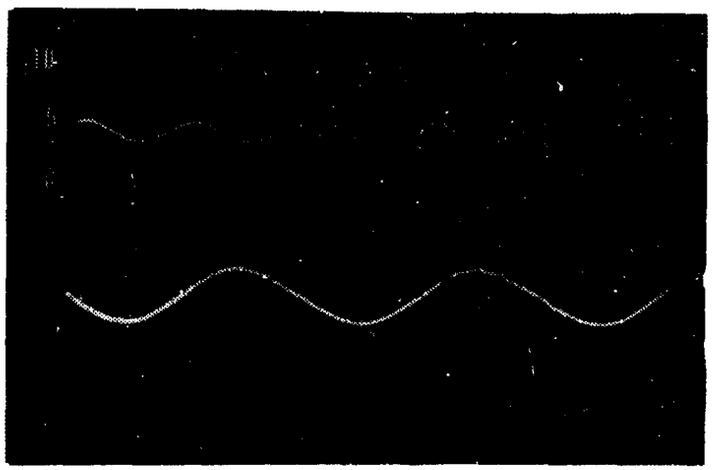

Sweep =
0.5 sec/cm

$r/r_o = 0.873$

Volts

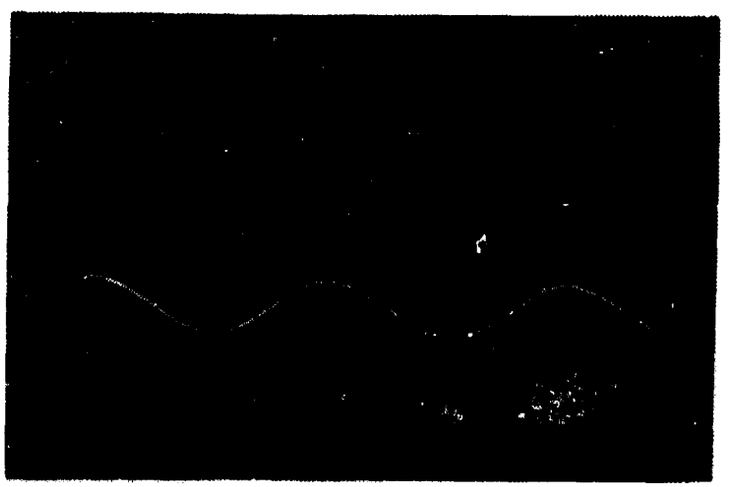

Sweep =
0.5 sec/cm

$r/r_o = 0.937$

Axial Velocity Distribution

Large Amplitude Pulse

Station #1

Volts

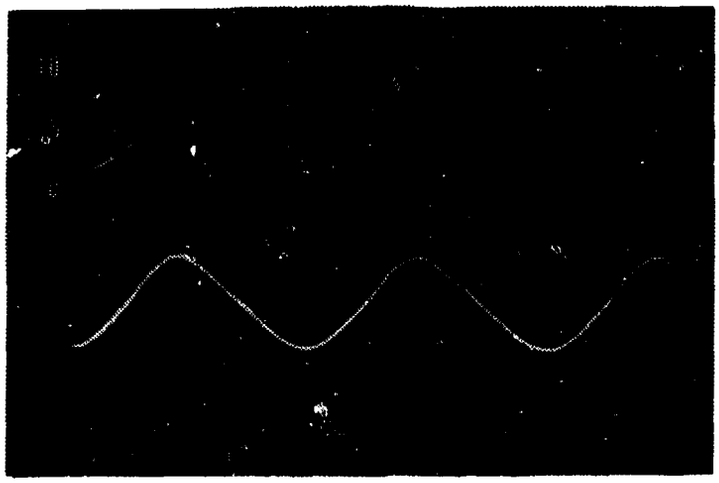

Sweep =
0.5 sec/cm

r/r_o = 0.00

Volts

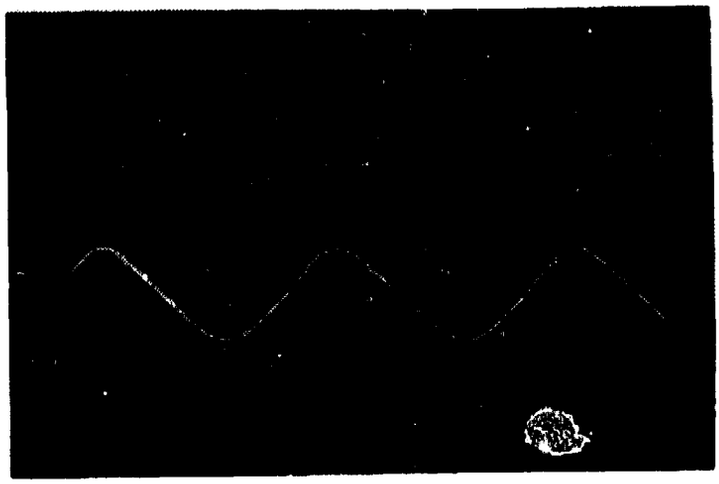

Sweep =
0.5 sec/cm

r/r_o = 0.238

Axial Velocity Distribution

Large Amplitude Pulse

Station #1

Volts

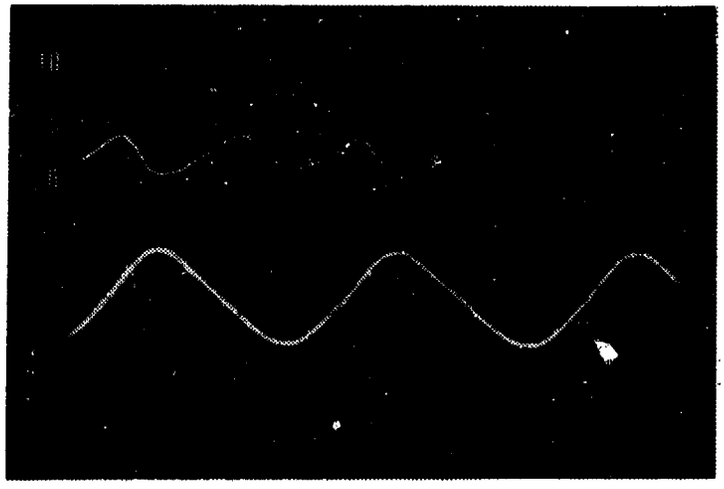

Sweep =
0.5 sec/cm

$r/r_o = 0.492$

Volts

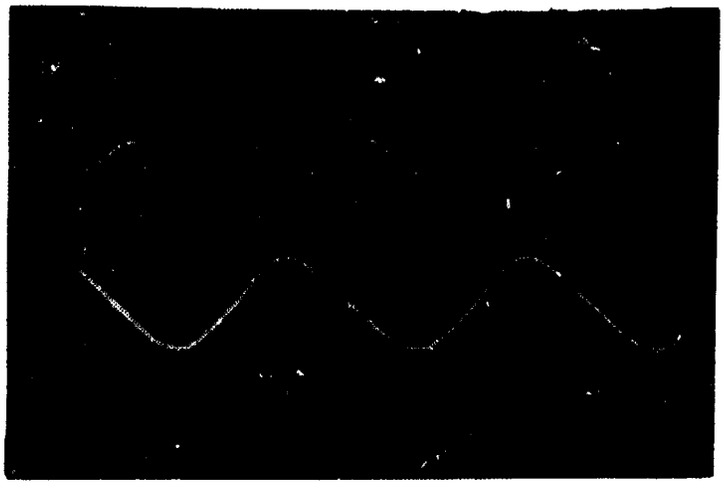

Sweep =
0.5 sec/cm

$r/r_o = 0.746$

Axial Velocity Distribution

Large Amplitude Pulse

Station #1

Volts

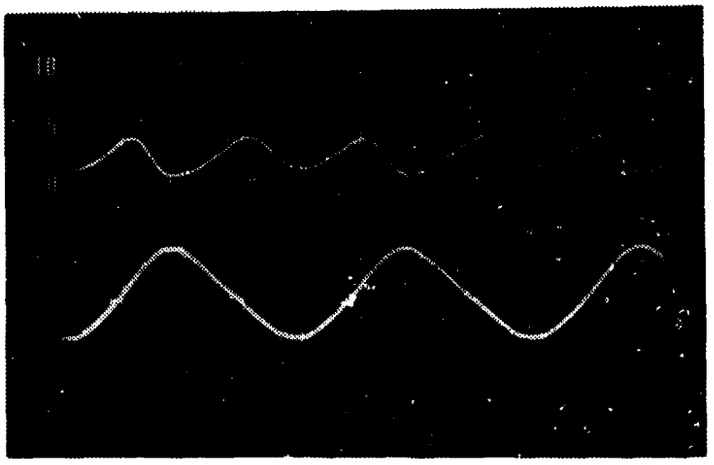

Sweep =
0.5 sec/cm

$r/r_o = 0.873$

Volts

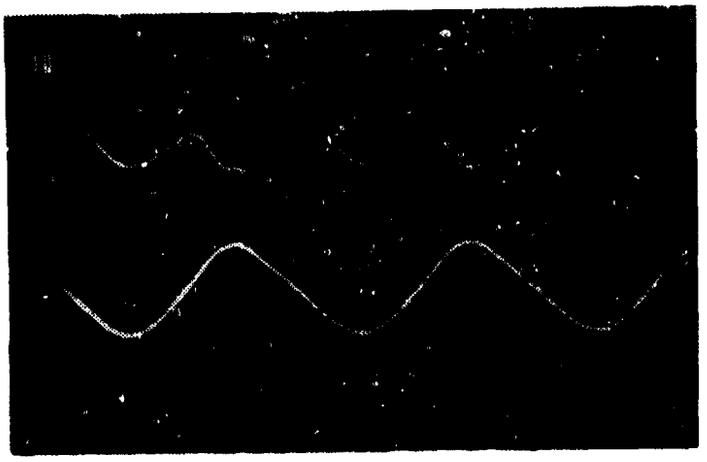

Sweep =
0.5 sec/cm

$r/r_o = 0.937$

Axial Velocity Distribution

Large Amplitude Pulse

Station #2

Volts

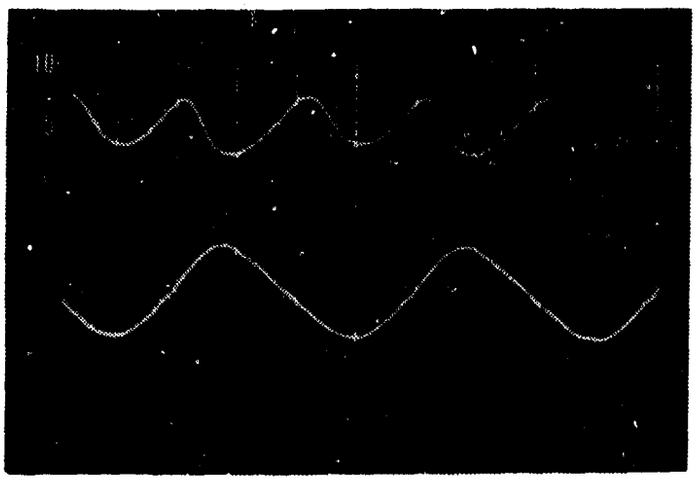

Sweep =
0.5 sec/cm

$r/r_o = 0.00$

Volts

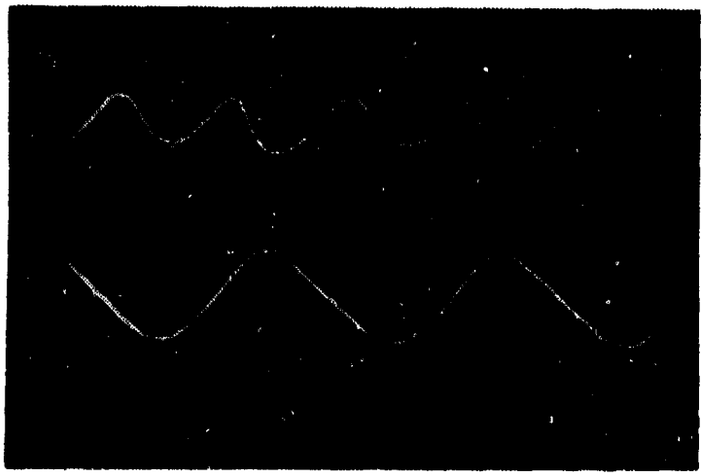

Sweep =
0.5 sec/cm

$r/r_o = 0.111$

Axial Velocity Distribution

Large Amplitude Pulse

Station #2

Volts

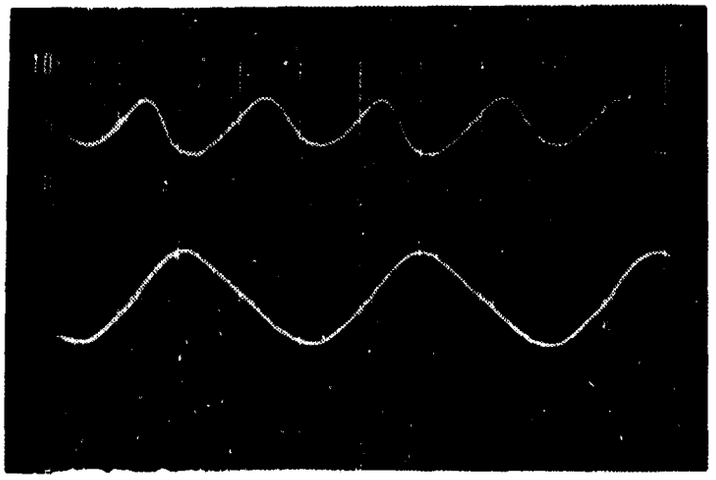

Sweep =
0.5 sec/cm

$r/r_o = 0.238$

Volts

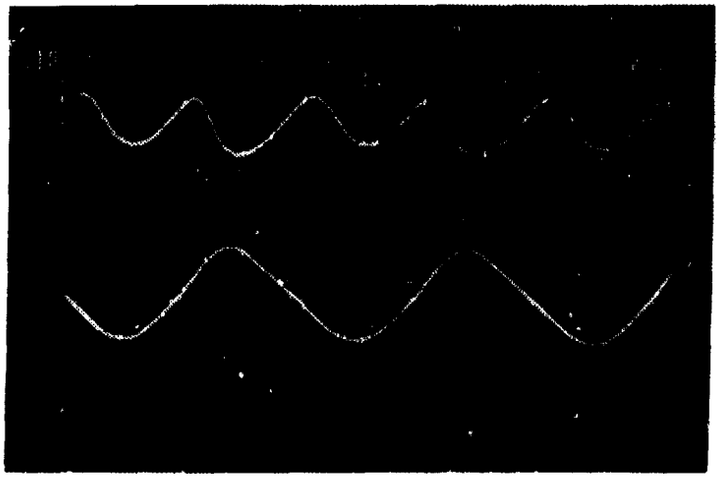

Sweep =
0.5 sec/cm

$r/r_o = 0.365$

Axial Velocity Distribution

Large Amplitude Pulse

Station #2

Volts

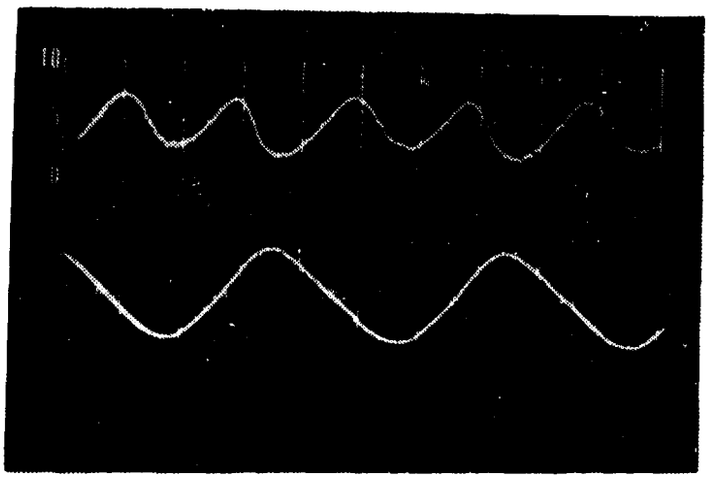

Sweep =
0.5 sec/cm

$r/r_o = 0.492$

Volts

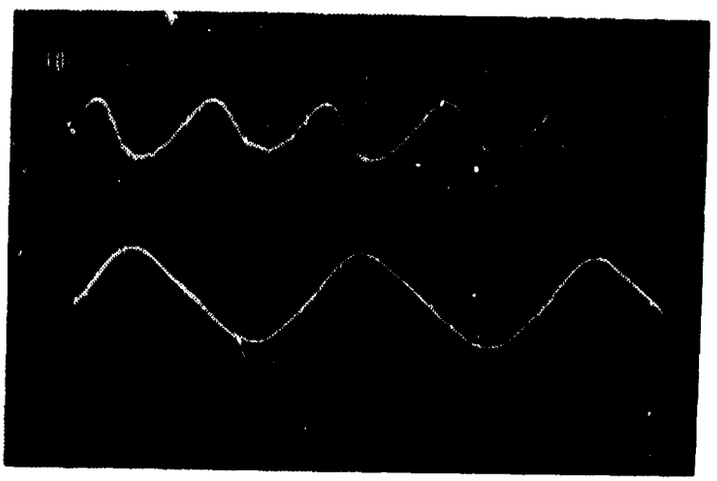

Sweep =
0.5 sec/cm

$r/r_o = 0.619$

Axial Velocity Distribution

Large Amplitude Pulse

Station #2

Volts

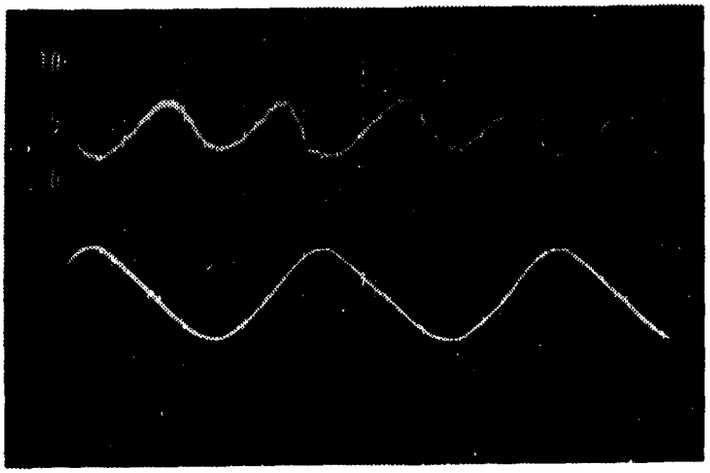

Sweep =
0.5 sec/cm

$r/r_o = 0.746$

Volts

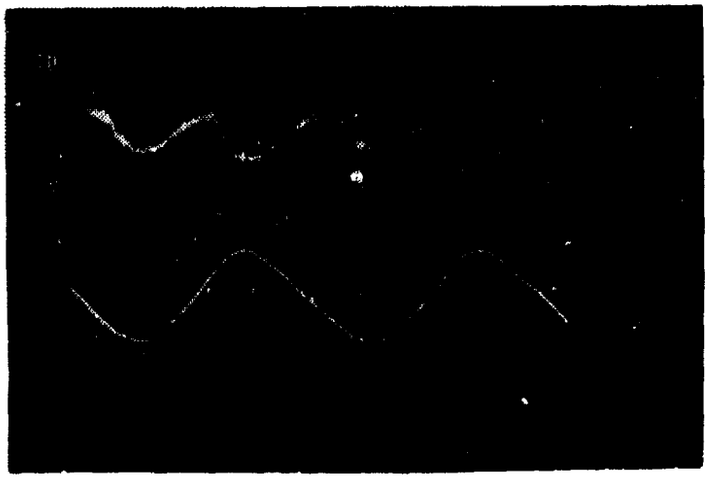

Sweep =
0.5 sec/cm

$r/r_o = 0.873$

Axial Velocity Distribution

Large Amplitude Pulse

Station #2

Volts

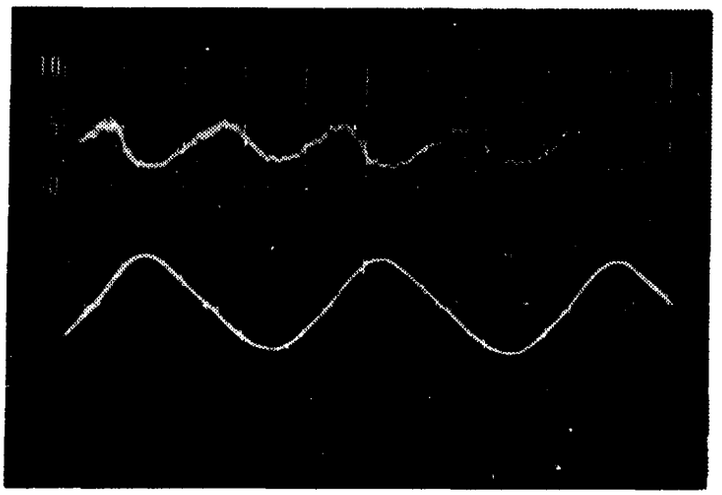

Sweep =
0.5 sec/cm

$r/r_o = 0.937$

Small Amplitude Pulse

Volts

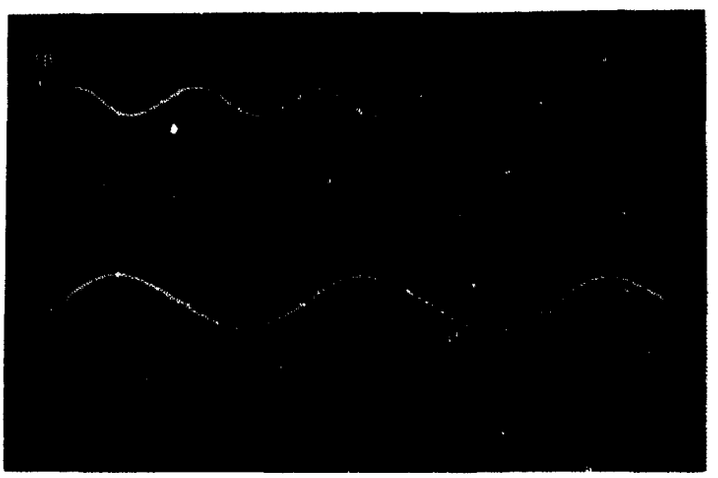

Sweep =
0.5 sec/cm

$r/r_o = 0.00$

Axial Velocity Distribution

Small Amplitude Pulse

Station #2

Volts

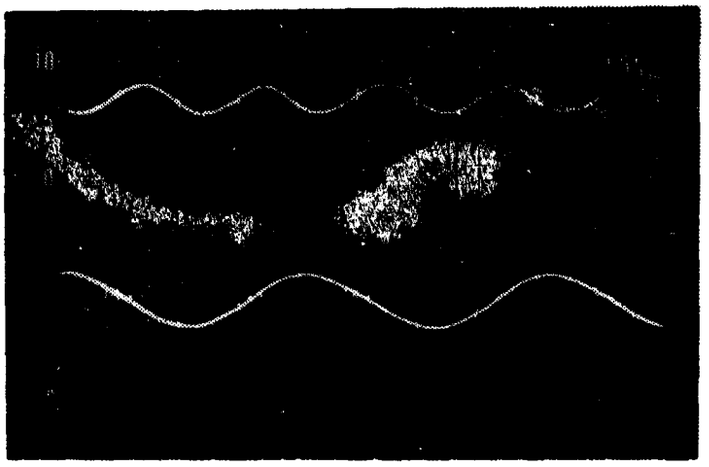

Sweep = 0.5 sec/cm

$r/r_o = 0.111$

Volts

Sweep = 0.5 sec/cm

$r/r_o = 0.238$

Axial Velocity Distribution

Small Amplitude Pulse

Station #2

Volts

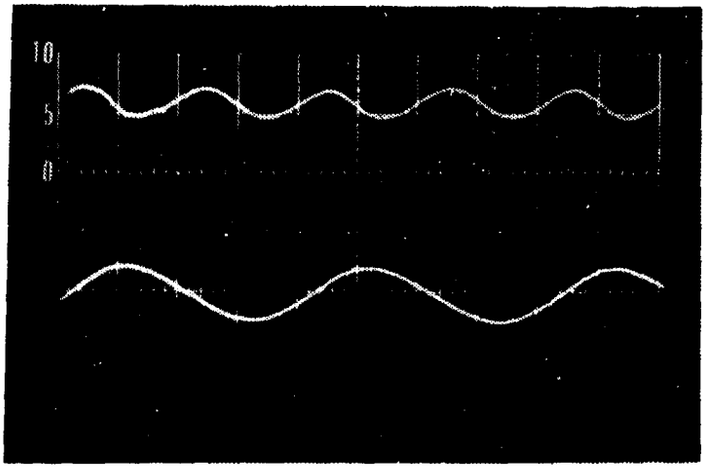

Sweep =
0.5 sec/cm

$r/r_o = 0.365$

Volts

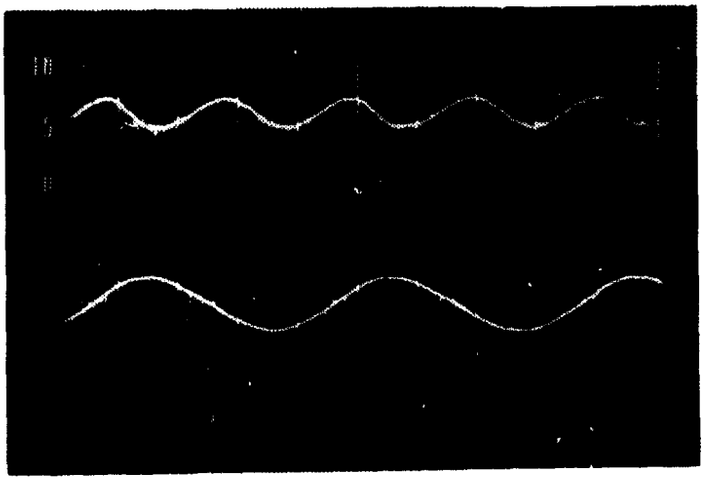

Sweep =
0.5 sec/cm

$r/r_o = 0.492$

Axial Velocity Distribution

Small Amplitude Pulse

Station #2

Volts

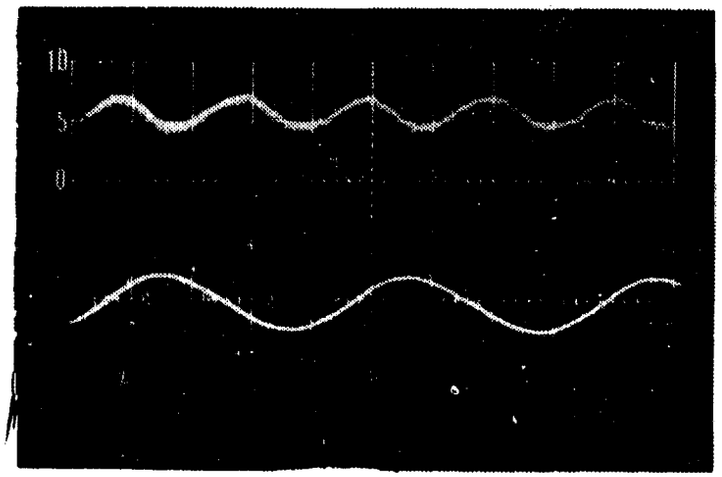

Sweep =
0.5 sec/cm

$r/r_o = 0.619$

Volts

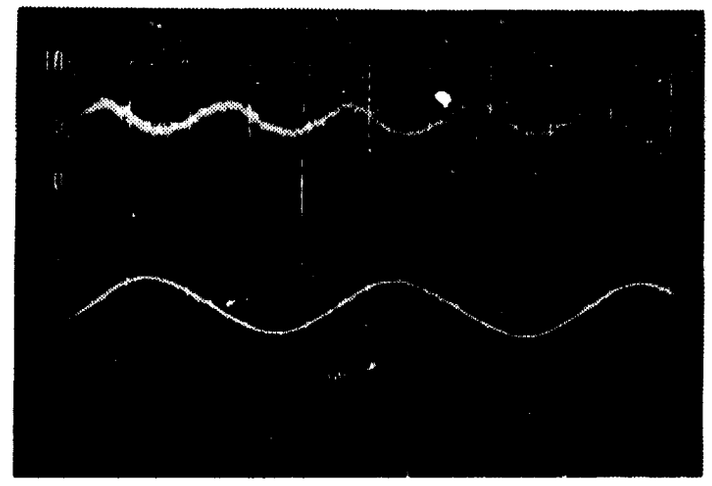

Sweep =
0.5 sec/cm

$r/r_o = 0.746$

Axial Velocity Distribution

Small Amplitude Pulse

Station #2

Volts

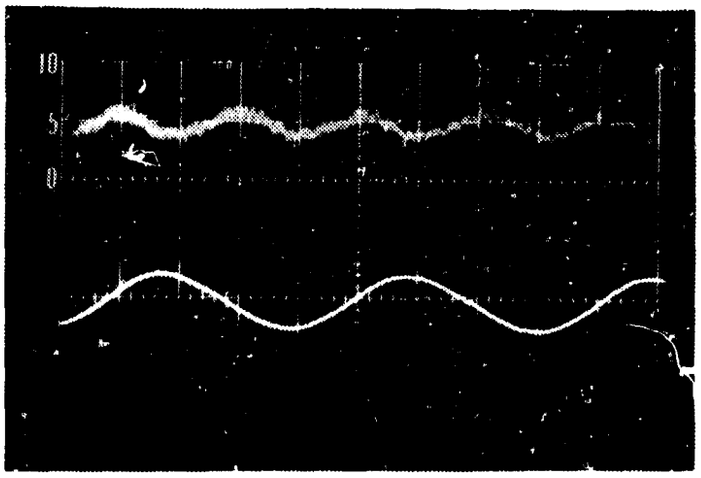

Sweep =
0.5 sec/cm

$r/r_o = 0.873$

Volts

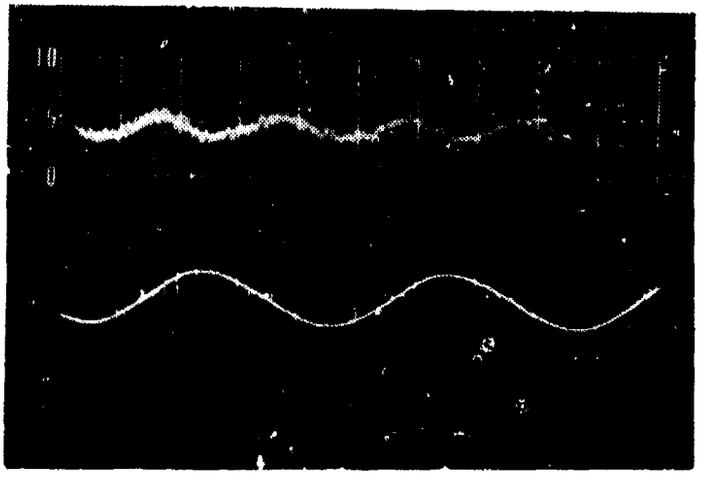

Sweep =
0.5 sec/cm

$r/r_o = 0.937$

Axial Velocity Distribution

Large Amplitude Pulse

Station #3

Volts

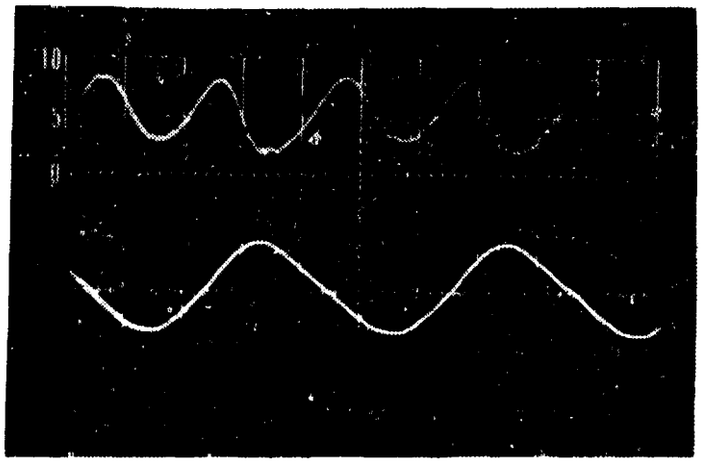

Sweep =
0.5 sec/cm

$r/r_o = 0.00$

Volts

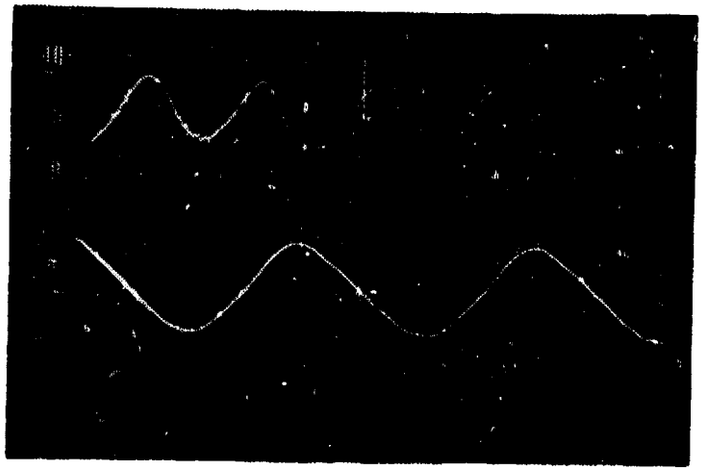

Sweep =
0.5 sec/cm

$r/r_o = 0.111$

Axial Velocity Distribution

Large Amplitude Pulse

Station #3

Volts

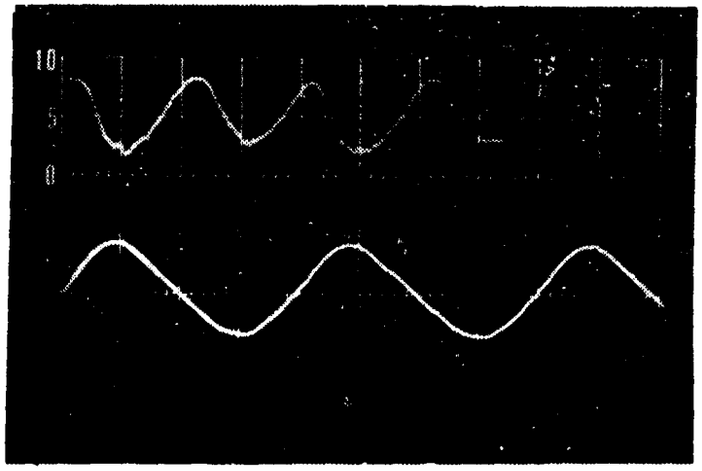

Sweep =
0.5 sec/cm

$r/r_o = 0.238$

Volts

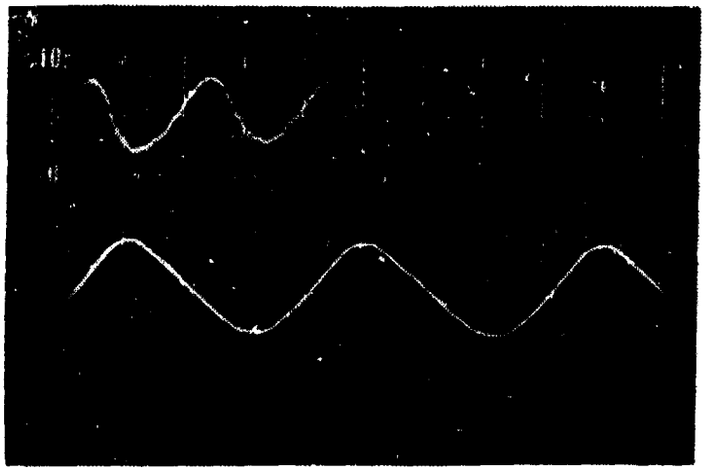

Sweep =
0.5 sec/cm

$r/r_o = 0.365$

Axial Velocity Distribution

Large Amplitude Pulse

Station #3

Volts

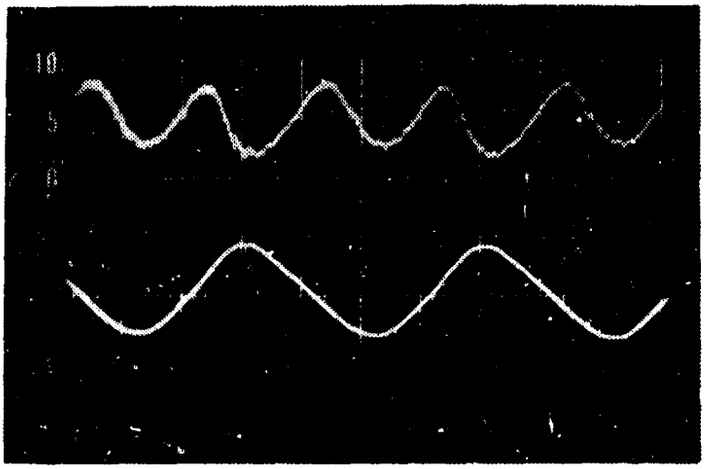

Sweep =
0.5 sec/cm

$r/r_o = 0.492$

Volts

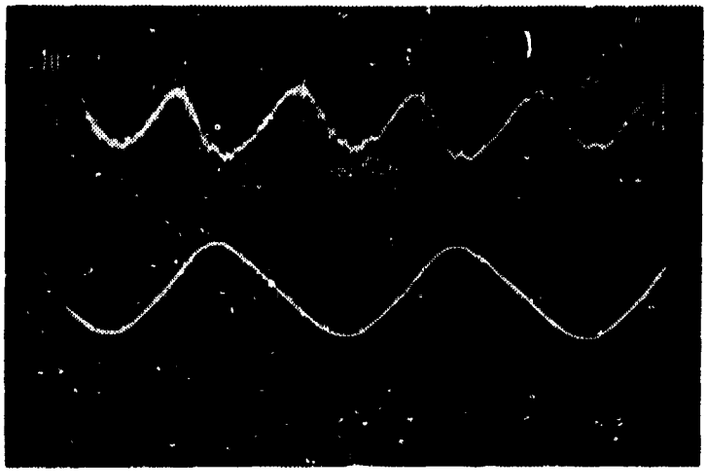

Sweep =
0.5 sec/cm

$r/r_o = 0.619$

Axial Velocity Distribution

Large Amplitude Pulse

Station #3

Volts

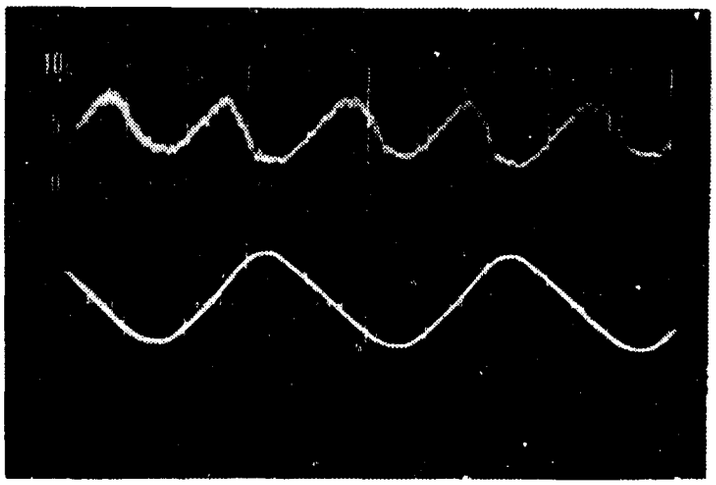

Sweep =
0.5 sec/cm

$r/r_o = 0.746$

Volts

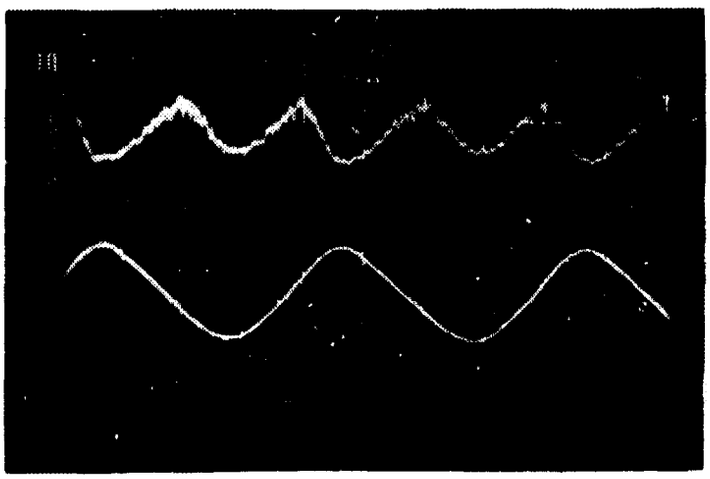

Sweep =
0.5 sec/cm

$r/r_o = 0.873$

Axial Velocity Distribution

Large Amplitude Pulse

Station #3

Volts

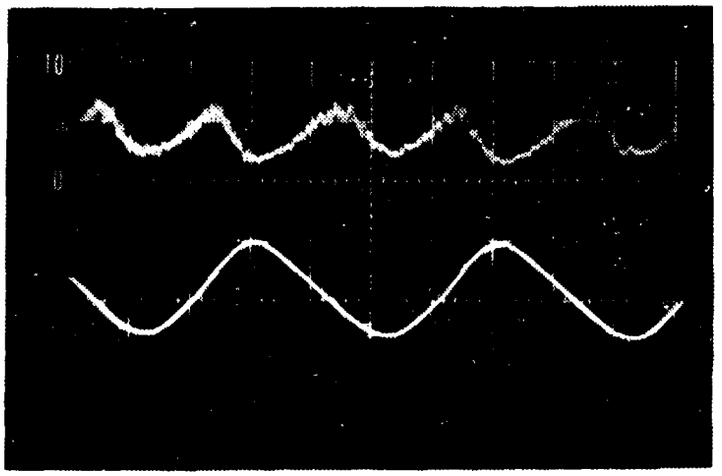

Sweep =
0.5 sec/cm

$r/r_o = 0.937$

Small Amplitude Pulse

Volts

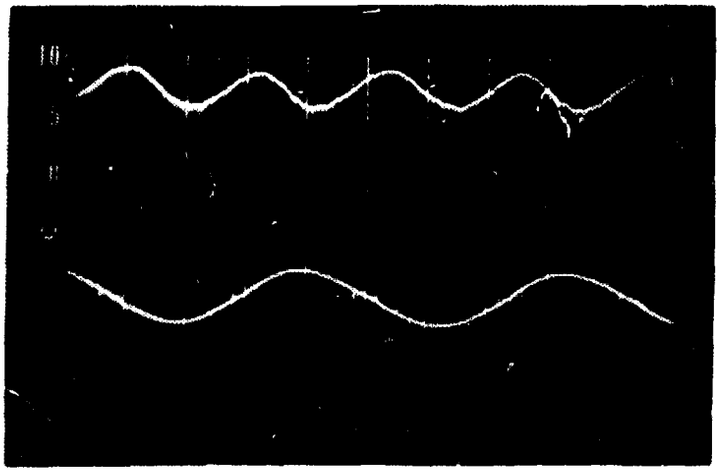

Sweep =
0.5 sec/cm

$r/r_o = 0.00$

Axial Velocity Distribution

Small Amplitude Pulse

Station #3

Volts

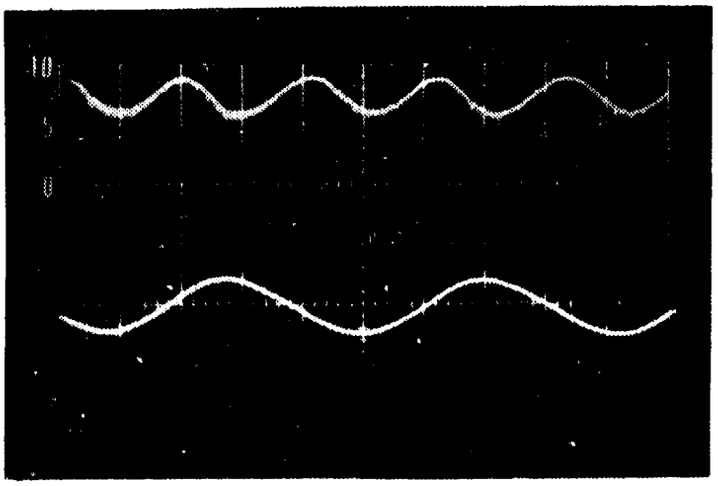

Sweep =
0.5 sec/cm

$r/r_o = 0.111$

Volts

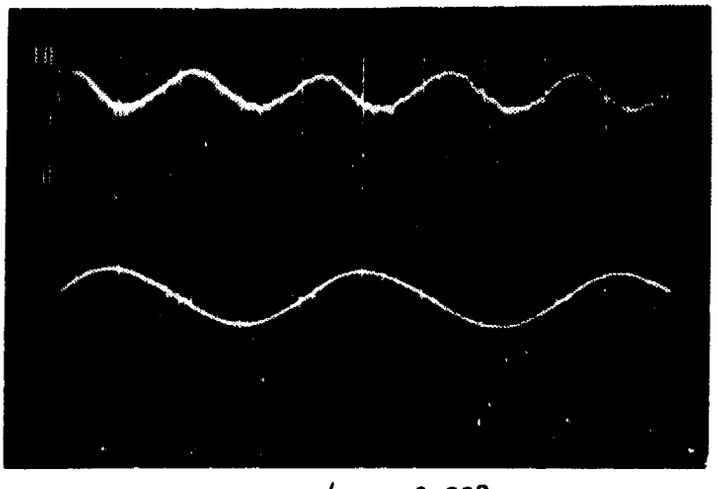

Sweep =
0.5 sec/cm

$r/r_o = 0.238$

Axial Velocity Distribution

Small Amplitude Pulse

Station #3

Volts

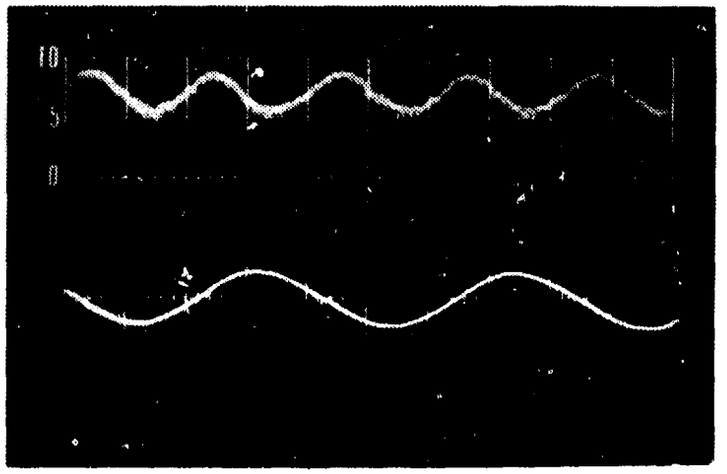

Sweep =
0.5 sec/cm

$r/r_o = 0.365$

Volts

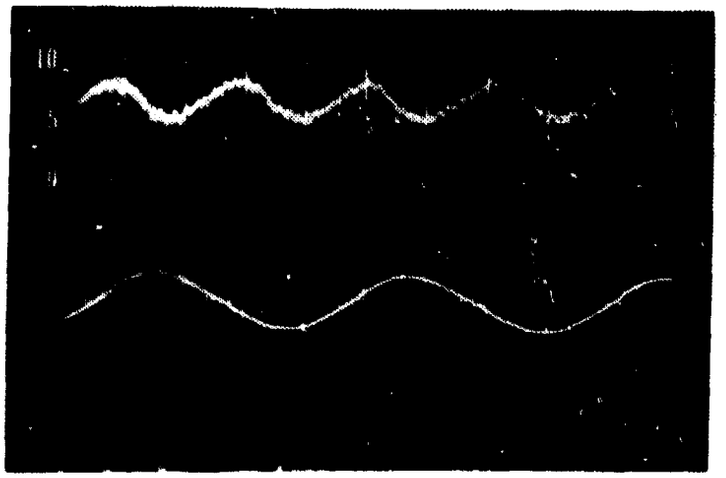

Sweep =
0.5 sec/cm

$r/r_o = 0.492$

Axial Velocity Distribution

Small Amplitude Pulse

Station #3

Volts

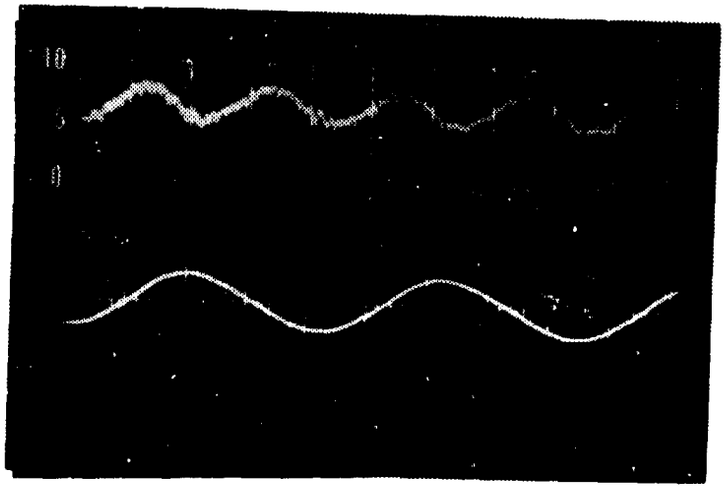

Sweep =
0.5 sec/cm

$r/r_o = 0.619$

Volts

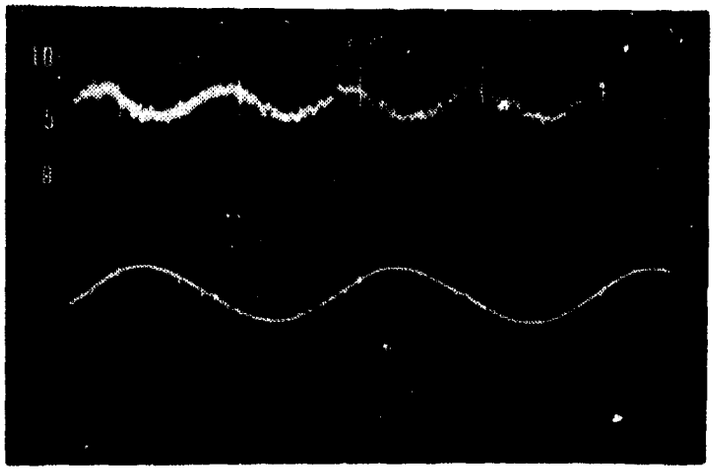

Sweep =
0.5 sec/cm

$r/r_o = 0.746$

Axial Velocity Distribution

Small Amplitude Pulse

Station #3

Volts

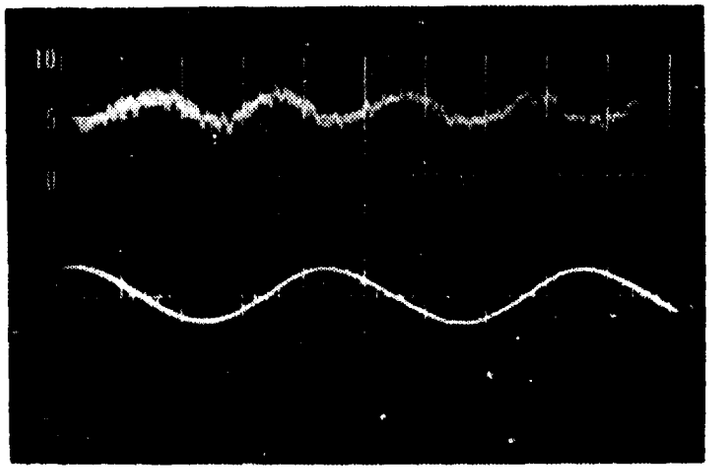

Sweep =
0.5 sec/cm

$r/r_o = 0.873$

Volts

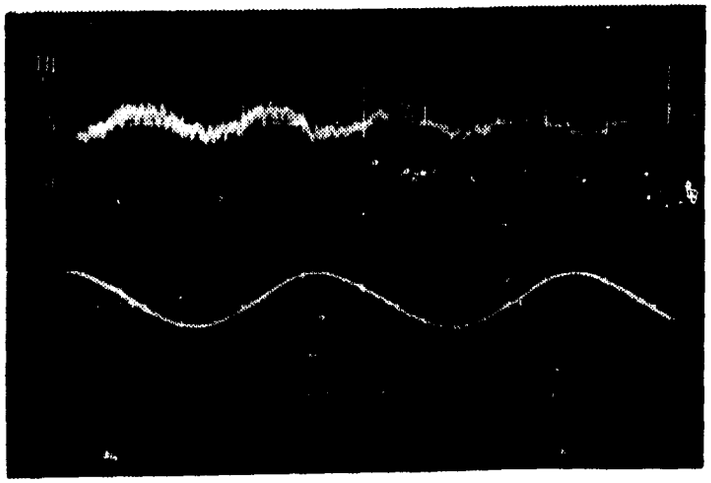

Sweep =
0.5 sec/cm

$r/r_o = 0.937$

Radial Velocity Distribution

Large Amplitude Pulse

Station #1

Volts
(x 10^2)

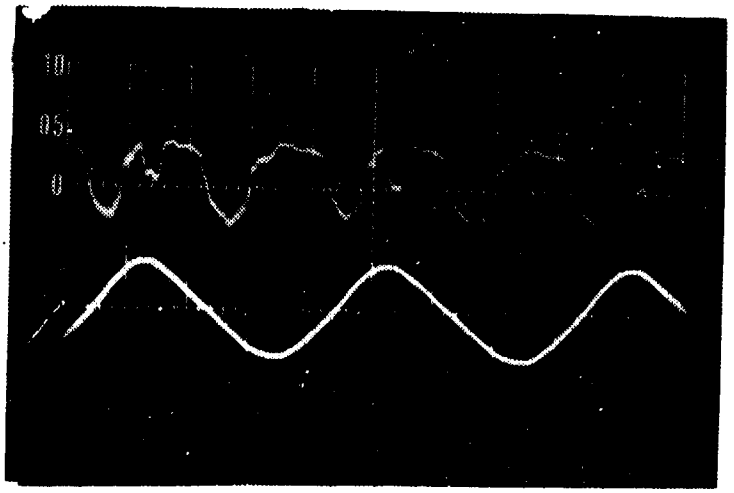

Sweep =
0.5 sec/cm

r/r_o = 0.00

Volts
(x 10^2)

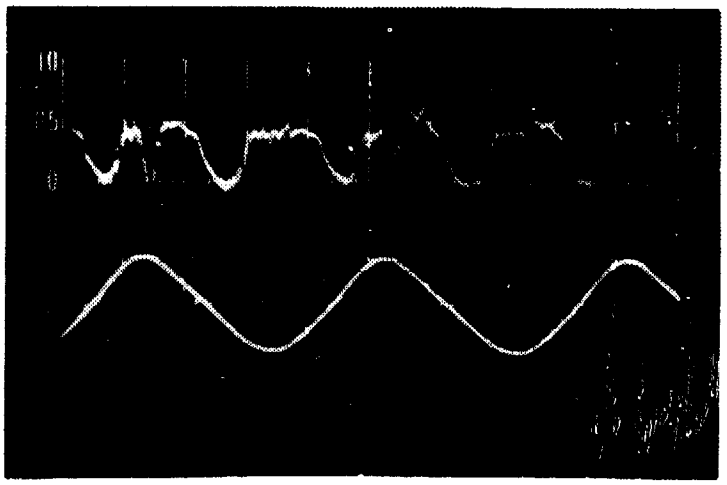

Sweep =
0.5 sec/cm

r/r_o = 0.492

Radial Velocity Distribution

Small Amplitude Pulse

Station #1

Volts
(x 10^2)

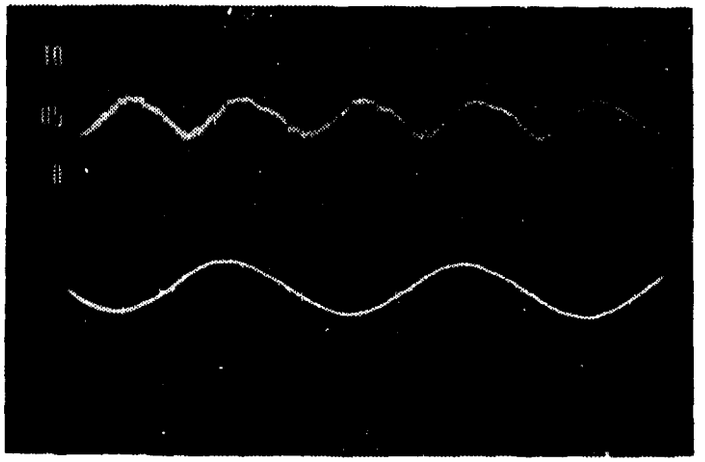

Sweep =
0.5 sec/cm

r/r_o = 0.00

Volts
(x 10^2)

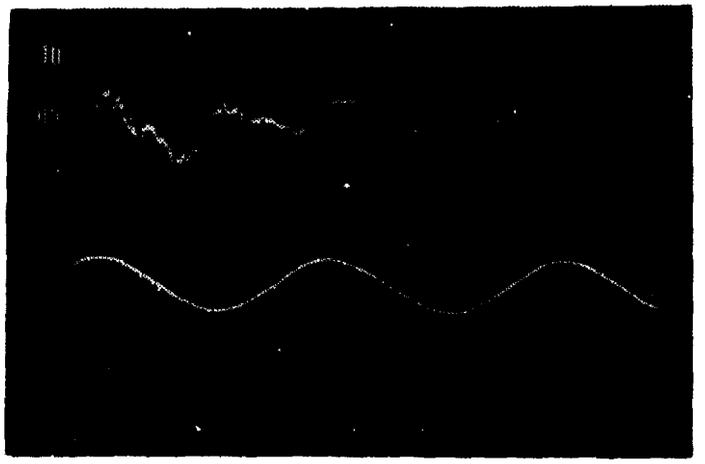

Sweep =
0.5 sec/cm

r/r_o = 0.492

Radial Velocity Distribution

Large Amplitude Pulse

Station #2

Volts
(x 10)

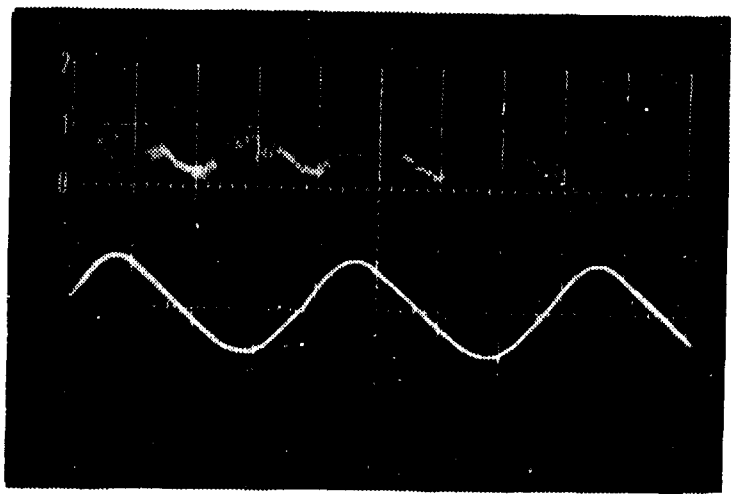

Sweep =
0.5 sec/cm

$r/r_o = 0.00$

Volts
(x 10)

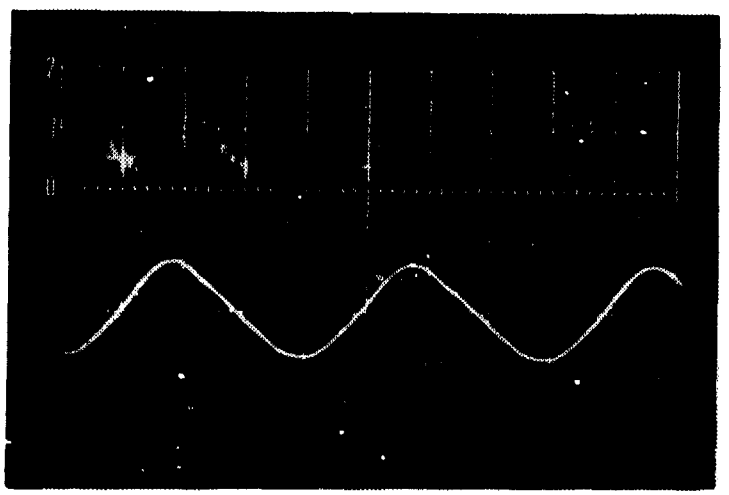

Sweep =
0.5 sec/cm

$r/r_c = 0.492$

Radial Velocity Distribution

Small Amplitude Pulse

Station #2

Volts
(x 10)

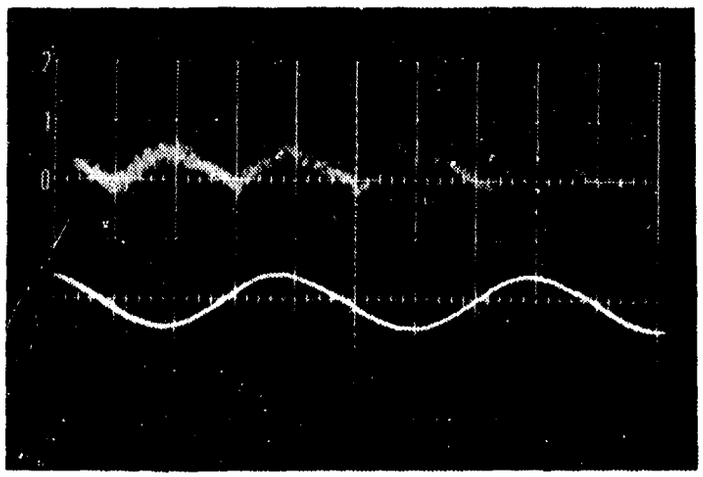

Sweep =
0.5 sec/cm

$r/r_o = 0.00$

Volts
(x 10)

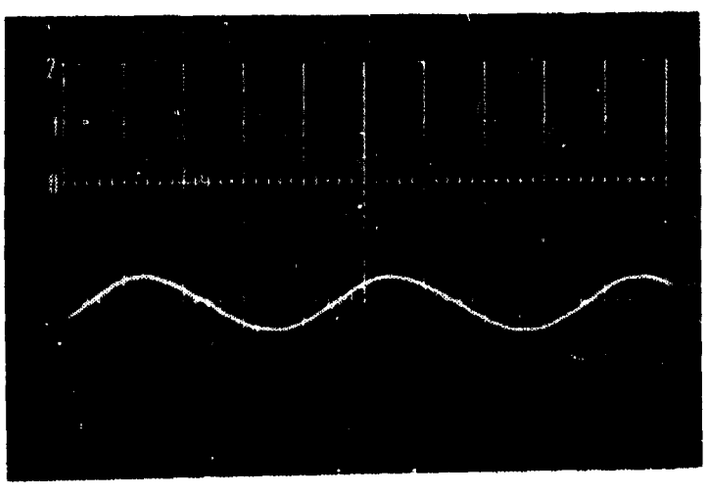

Sweep =
0.5 sec/cm

$r/r_o = 0.492$

Radial Velocity Distribution

Large Amplitude Pulse

Station #3

Volts
(x 10)

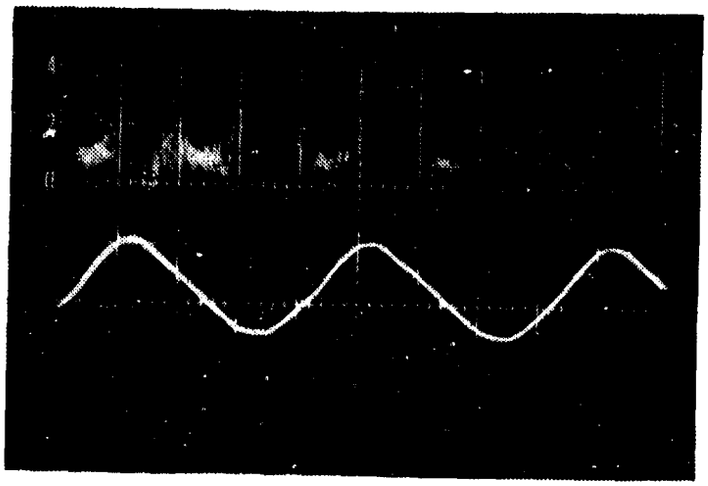

Sweep =
0.5 sec/cm

$r/r_o = 0.00$

Volts
(x 10)

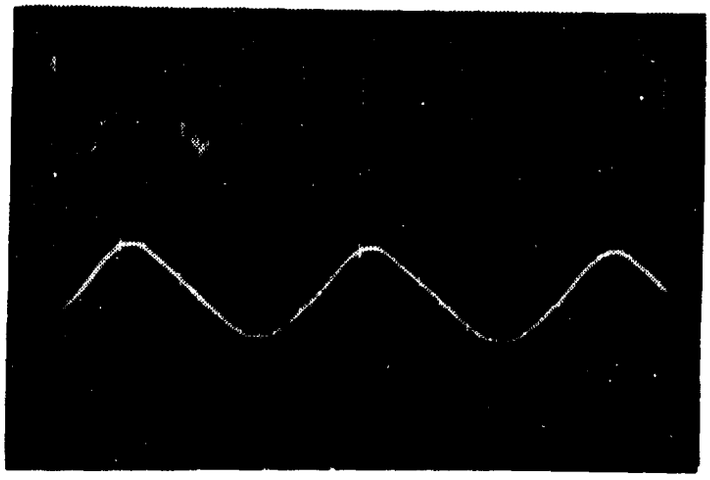

Sweep =
0.5 sec/cm

$r/r_o = 0.492$

Radial Velocity Distribution

Small Amplitude Pulse

Station #3

Volts
(x 10)

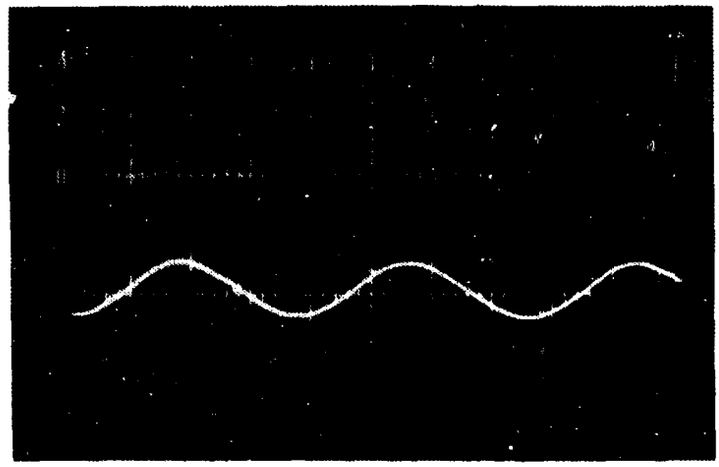

Sweep =
0.5 sec/cm

$r/r_o = 0.00$

Volts
(x 10)

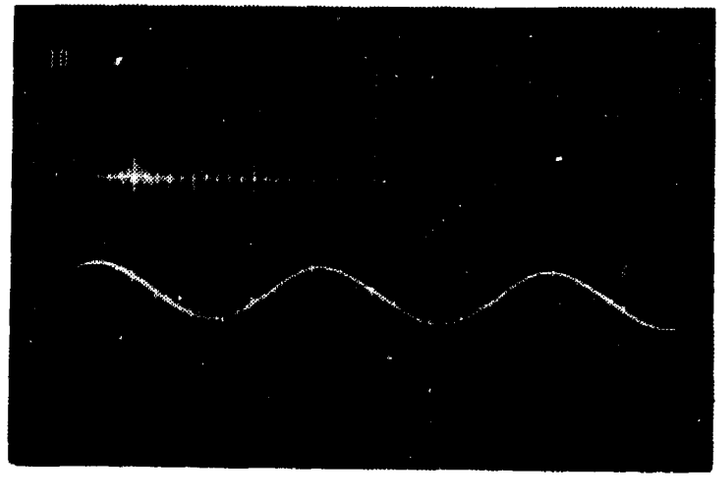

Sweep =
0.5 sec/cm

$r/r_o = 0.492$

APPENDIX E

MANOMETER DATA

Steady and Swirling Flow

(P_t=30.04 in. Hg)

x (dia)	Steady Flow Δh (in. H_2O)	Steady Flow ΔP (psf)	Large Swirl Δh (in. H_2O)	Large Swirl ΔP (psf)	Small Swirl Δh (in. H_2O)	Small Swirl ΔP (psf)
0.75	3.85	10.01	3.70	9.62	3.70	9.62
2.25	3.90	10.14	3.75	9.75	3.80	9.88
3.75	4.05	10.53	3.95	10.27	4.00	10.40
5.25	4.05	10.53	4.0	10.40	4.05	10.53
6.75	4.15	10.79	4.05	10.53	4.10	10.66
8.25	4.25	11.05	4.15	10.79	4.20	10.92
9.75	4.40	11.44	4.30	11.18	4.35	11.31
11.25	4.45	11.57	4.40	11.44	4.40	11.44
12.75	4.75	12.35	4.75	12.35	4.75	12.35
14.25	4.85	12.61	4.85	12.61	4.85	12.61
15.75	4.65	12.09	4.55	11.83	4.55	11.83
17.25	4.95	12.87	4.85	12.61	4.90	12.79
18.75	4.85	12.61	4.80	12.48	4.80	12.48
20.25	4.90	12.74	4.90	12.74	4.90	12.74
21.75	4.95	12.87	4.95	12.87	4.95	12.87
23.25	5.00	13.00	5.00	13.00	4.95	12.87
24.75	5.10	13.26	5.10	13.26	5.10	13.26
26.25	5.25	13.65	5.30	13.78	5.30	13.78
27.75	5.25	13.65	5.25	13.65	5.25	13.65

Steady and Swirling Flow (cont.)

x (dia)	Steady Flow Δh (in. H_2O)	Steady Flow Δp (psf)	Large Swirl Δh (in. H_2O)	Large Swirl Δp (psf)	Small Swirl Δh (in. H_2O)	Small Swirl Δp (psf)
29.25	5.30	13.78	5.35	13.91	5.35	13.91
30.75	5.60	14.56	5.65	14.69	5.65	14.69
32.25	5.55	14.43	5.60	14.56	5.55	14.43
33.75	5.70	14.82	5.80	15.08	5.75	14.95
35.25	5.55	14.43	5.65	14.69	5 60	14.56
36.75	5.70	14.82	5.80	15.08	5.75	14.95
38.25	5.70	14.82	5.85	15.21	5.80	15.08
39.75	5.85	15.21	5.95	15.47	5.95	15.47
41.25	5.95	15.47	0.00	15.60	6.00	15.60
42.75	5.95	15.47	6.05	15.73	6.05	15.73
44.25	6.15	15.99	6.25	16.25	6.20	16.12
45.75	6.05	15.73	6.15	15.99	6.10	15.86
47.25	6.25	16.25	6.45	16.77	6.35	16.51
48.75	6.20	16.12	6.35	16.51	6.30	16.38
50.25	6.35	16.51	6.50	16.90	6.45	16.77

Pulsing Flow

(P_t = 30.04 in Hg)

x (dia)	Small Amplitude $(\Delta h)_{ave}$ (in. H_2O)	Small Amplitude $(\Delta p)_{ave}$ (psf)	Large Amplitude $(\Delta h)_{ave}$ (in. H_2O)	Large Amplitude $(\Delta p)_{ave}$ (psf)
0.75	2.63	6.83	1.70	4.42
2.25	2.68	6.96	1.75	4.55
3.75	2.73	7.09	1.80	4.68
5.25	2.73	7.09	1.78	4.62
6.75	2.78	7.22	1.83	4.75
8.25	2.83	7.35	1.88	4.88
9.75	2.93	7.61	1.90	4.94
11.25	2.95	7.67	1.93	5.01
12.75	3.08	8.00	1.98	5.14
14.25	3.20	8.32	2.03	5.27
15.75	3.08	8.00	1.98	5.14
17.25	3.23	8.39	2.03	5.27
18.75	3.18	8.26	2.03	5.27
20.25	3.23	8.39	2.03	5.27
21.75	3.25	8.45	2.05	5.33
23.25	3.30	8.58	2.08	5.40
24.75	3.33	8.65	2.10	5.46
26.25	3.38	8.78	2.13	5.53
27.75	3.33	8.65	2.13	5.53

Pulsing Flow (cont.)

x (dia)	Small Amplitude $(\Delta h)_{ave}$ (in. H_2O)	Small Amplitude $(\Delta p)_{ave}$ (psf)	Large Amplitude $(\Delta h)_{ave}$ (in. H_2O)	Large Amplitude $(\Delta p)_{ave}$ (psf)
29.25	3.40	8.84	2.15	5.59
30.75	3.50	9.10	2.25	5.85
32.25	3.38	9.17	2.23	5.79
33.75	3.65	9.49	2.25	5.85
35.25	3.58	9.30	2.25	5.85
36.75	3.65	9.49	2.25	5.85
38.25	3.68	9.56	2.30	5.98
39.75	3.75	9.75	2.30	5.98
41.25	3.85	10.01	2.35	6.11
42.75	3.80	9.88	2.35	6.11
44.25	3.99	10.14	2.40	6.24
45.75	3.90	10.14	2.40	6.24
47.25	4.03	10.47	2.43	6.31
48.75	3.98	10.34	2.43	6.31
50.25	4.08	10.60	2.45	6.37

APPENDIX F

WALL STATIC PRESSURE TRANSDUCER DATA

Station #1

Volts
($\times 10^{3}$)

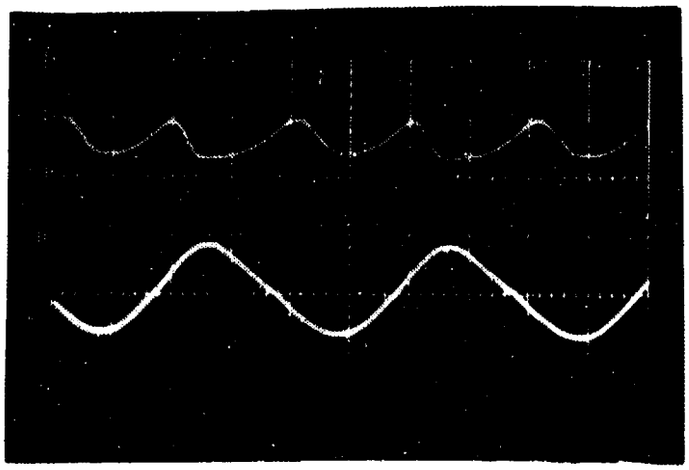

Sweep =
0.5 sec/cm

Large Amplitude Pulse

Volts
($\times 10^{4}$)

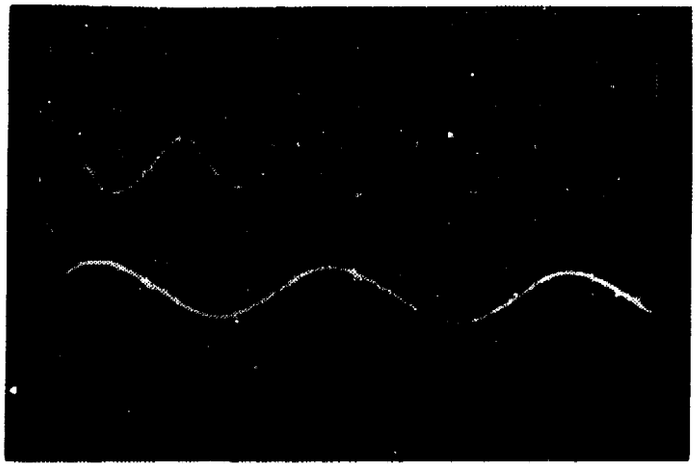

Sweep =
0.5 se 'cm

Small Amplitude Pulse

Station #2

Volts
(x 10^{3})

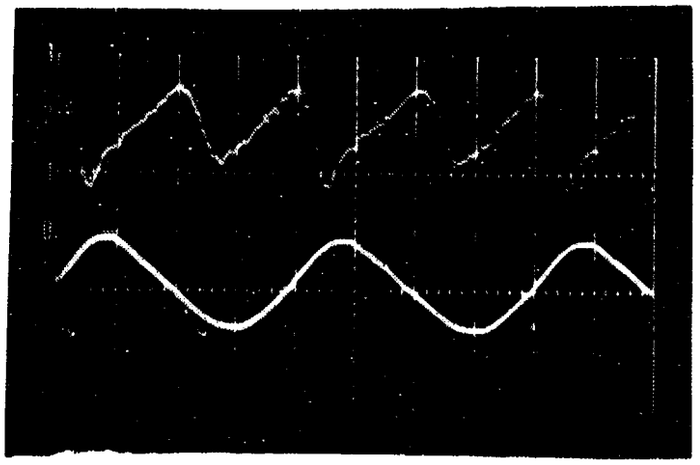

Sweep =
0.5 sec/cm

Large Amplitude Pulse

Volts
(x 10^{4})

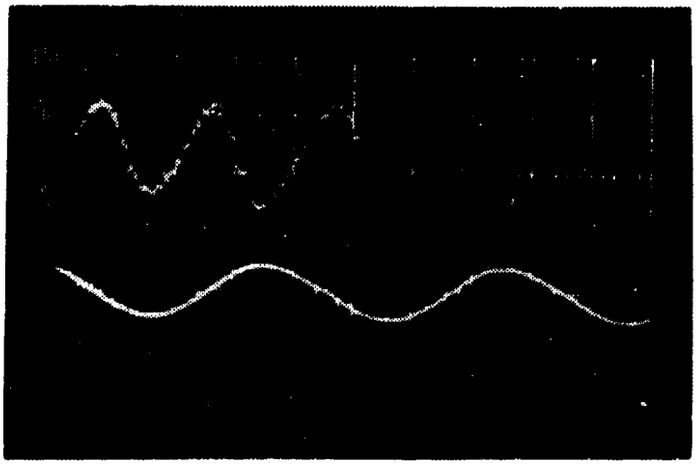

Sweep =
0.5 sec/cm

Small Amplitude Pulse

Station #3

Volts
(x 10^3)

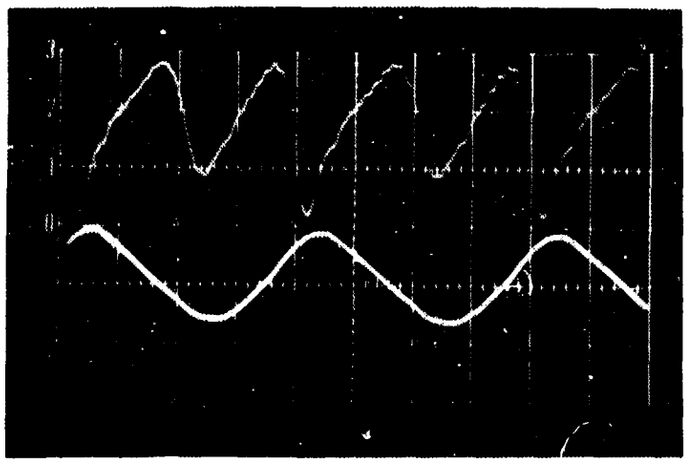

Sweep =
0.5 sec/cm

Large Amplitude Pulse

Volts
(x 10^4)

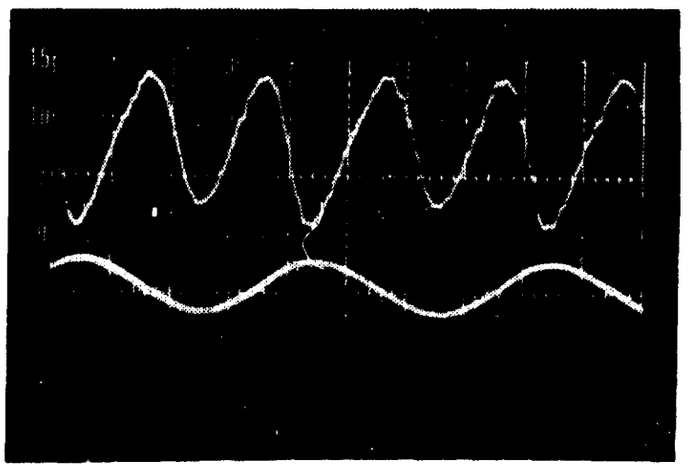

Sweep =
0.5 sec/cm

Small Amplitude Pulse

LIST OF REFERENCES

1. Hagen, G., "Über die Bewegung des Wassers in engen zylindrischen Röhren," in Schlichting, Boundary Layer Theory, p. 12.

2. Poiseuille, J., "Récherches expérimentelles sur le mouvement des liquides dans les tubes de très petits diamètres," in Schlichting, Boundary Layer Theory, p. 12.

3. Reynolds, O., "On the Dynamic Theory of Incompressible Viscous Fluids and the Determination of the Criterion," in Schlichting, Boundary Layer Theory, p. 432.

4. Blasius, H., "Das Ähnlichkeitsgesetz bei Reibungsvorgängen in Flussigkeiten," in Schlichting, Boundary Layer Theory, p. 561.

5. Prandtl, L., "The Mechanics of Viscous Fluids," in Schlichting, Boundary Layer Theory, p. 572-574.

6. Nikuradse, J., "Gesetzmassigkeit der turbulenten Strömung in glatten Rohren," in Schlichting, Boundary Layer Theory, p. 574.

7. Aerospace Research Laboratories, ARL 71-0244, Survey of Some Aspects of Swirling Flows, by S.N.B. Murthy, November 1971.

8. Aerospace Research Laboratories, ARL 66-0083, Investigation of Swirling Flows in Ducts, by Z. Lavan and A. A. Fejer, May 1966.

9. National Aeronautics and Space Administration, CR-1169, Analytical Investigation of Incompressible Turbulent Swirling Flow in Pipes, by A. P. Rochino and Z. Lavan, September 1968.

10. Jet Propulsion Center, Purdue University, F-67-9, An Analytical and Experimental Investigation of Swirling Flow in Nozzles, by D. J. Norton, B. W. Farquhar and J. D. Hoffman, October 1967.

11. Jet Propulsion Center, Purdue University, TM-67-8, An Experimental Investigation of Swirling Flow in Nozzles, by B. W. Farquhar, D. J. Norton and J. D. Hoffman, January 1968.

12. Sexl, T., "Über den von E. G. Richardson entdeckten 'Annulareffekt'," in Schlichting, Boundary Layer Theory, p. 419.

13. Uchida, S., "The Pulsating Viscous Flow Superimposed on the Steady Laminar Motion of Incompressible Fluid in a Circular Pipe," Zeitschrift für angewandte Mathematik und Physik, v. 7, p. 403-422, 1956.

14. National Aeronautics and Space Administration, TN-D-6213, Randomly Fluctuating Flow in a Channel Due to Randomly Fluctuating Pressure Gradients, by M. Perlmutter, March 1971.

BIBLIOGRAPHY

1. Aerospace Research Laboratories, ARL 66-0083, Investigation of Swirling Flows in Ducts, by Z. Lavan and A.A. Fejer, May 1966.

2. Aerospace Research Laboratories, ARL 71-0244, Survey of Some Aspects of Swirling Flows, by S.N.B. Murthy, November 1971.

3. Edwards, M. F., and W. L. Wilkenson, "Review of Potential Applications of Pulsating Flow in Pipes," Transactions of the Institution for Chemical Engineers, v. 49, 1971.

4. General Electric Space Sciences Laboratory, R66SD61, Exact Solutions to the Navier-Stokes Equations with Curl Free Convective Accelerations, by S. Weinbaum and V. O'Brien, September 1966.

5. Jet Propulsion Center, Purdue University, F-67-9, An Analytical and Experimental Investigation of Swirling Flow in Nozzles, by D. J. Norton, B. W. Farquhar and J. D. Hoffman, October 1967.

6. Jet Propulsion Center, Purdue University, TM-67-8, An Experimental Investigation of Swirling Flow in Nozzles, by B. W. Farquhar, D. J. Norton and J. D. Hoffman, January 1968.

7. National Aeronautics and Space Administration, CR-990, Transient Behavior of Arterial Systems in Response to Flow Pulses, by E. D. Young, December 1967.

8. National Aeronautics and Space Administration, CR-1169, Analytical Investigation of Incompressible Turbulent Swirling Flow in Pipes, by A. P. Rochino and Z. Lavan, September 1968.

9. National Aeronautics and Space Administration, CR-1956, Some Effects of Swirl on Turbulent Mixing and Combustion, by A. Rubel, February 1972.

10. National Aeronautics and Space Administration, TN-D-6213, Randomly Fluctuating Flow in a Channel Due to Randomly Fluctuating Pressure Gradients, by M. Perlmutter, March 1971.

11. Schlichting, H., Boundary Layer Theory, McGraw-Hill Book Co., 1968.

12. Uchida, S., "The Pulsating Viscous Flow Superimposed on the Steady Laminar Motion of Incompressible Fluid in a Circular Pipe," Zeitschrift für angewandte Mathematik und Physik, v. 7, p. 403-422, 1956.

13. United Aircraft Research Laboratory, A Comparison of Theory and Experiment for Incompressible, Turbulent, Swirling Flows in Axisymmetric Ducts, by O. L. Anderson, February 1972.

14. Wood, W. W., "Calculations for Anemometry with Fine Hot Wires," Journal of Fluid Mechanics, v. 32, p. 9-19, 1968.